ISBN 978-82-326-4423-0 (printed version)
ISBN 978-82-326-4427-8 (electronic version)
ISSN 1503-8181

Doctoral theses at NTNU, 2020:30

Anisa Noor Corina

Cement Plug Integrity for Well Abandonment

NTNU
Norwegian University of
Science and Technology
Faculty of Engineering
Department of Geoscience and Petroleum

NTNU
Norwegian University of
Science and Technology

Doctoral theses at NTNU, 2020:30

NTNU

NTNU
Norwegian University of
Science and Technology

Anisa Noor Corina

Cement Plug Integrity for Well Abandonment

Thesis for the degree of Philosophiae Doctor

Trondheim, January 2020

Norwegian University of Science and Technology
Faculty of Engineering
Department of Geoscience and Petroleum

NTNU
Norwegian University of
Science and Technology

NTNU
Norwegian University of Science and Technology

Thesis for the degree of Philosophiae Doctor

Faculty of Engineering
Department of Geoscience and Petroleum

ISBN 978-82-326-4423-0 (printed version)
ISBN 978-82-326-4427-8 (electronic version)
ISSN 1503-8181

Doctoral theses at NTNU, 2020:30

Printed by Skipnes Kommunikasjon as

Summary

Permanent abandonment marks the end of the life of an oil or gas well. Accordingly, the penetrated formation must be isolated, preventing fluid flow to the surface or surrounding formation, with a purpose to give long-term environmental protection. The isolation is generally achieved by placing qualified sealing material, commonly cement, in the wellbore at specific intervals. Recently, there have been concerns about the sealing performance of the cement plug to create lasting isolation, knowing that the cement hydraulic integrity could be compromised under various conditions one can encounter downhole. Therefore, enhanced insight about cement plug sealing could provide the possibility to improve the planning and design of well abandonment operations in reducing the risk of integrity issues in plugged wells.

A laboratory test assessing the sealing ability of a material to a pipe can be a relevant approach for analyzing the hydraulic integrity of the cement plug. A literature study reveals that there were only a few numbers of experimental studies investigating sealing performance of cement plug, and the outcomes were dispersed and fragmented due to the lack of consistent experimental setup. This highlights that further investigations may be sought to yield additional information on the hydraulic integrity of cement plugs.

This research work aims to evaluate the sealing performance of cement plugs for permanent well abandonment by using a function test apparatus, constructed in the SINTEF laboratory. The test setup is based on the design from an existing study, which was also adopted in one of the Oil and Gas UK guidelines. It is a small-scale replica of a downhole system constituted of a cement plug enclosed inside a pipe. It has unique features that allow uninterrupted consecutive processes of curing and testing, and it can simulate the realistic downhole condition. In principle, the test is performed by subjecting a differential pressure and a flowing gas across a cement plug placed inside a test cell. The gas flow rate through the cement plug is measured and used as an indicator if the hydraulic sealing of the cement plug is compromised. The differential pressure during the first sign of a leak is also measured.

First, a preliminary test is conducted to examine the setup functionality, generate the baseline results, and compare cement curing conditions in results reproducibility. As the setup is found to be operational and the dry-curing method (i.e. curing without access to external water) is set in the testing protocol, comparative experiments are subsequently conducted. In these experiments, two cement systems of neat- and silica-based cement are tested with investigated parameters of pipe surface roughness, curing temperature, and cement additives. The results show that placement of the cement plugs next to a rough-surface pipe and addition

of expanding agents are both effective in reducing the gas leak rate, and they can be implemented to improve the integrity of the cement plug.

As the experimental results observed that leak was likely to occur at the microannulus between cement and pipe interface, this research work covers the investigation of the fluid flow dynamics in microannuli. The fluid dynamic study is conducted by using numerical simulation of computational fluid dynamics (CFD) and divided into two parts. The first part investigates the fluid flow dynamics of three fluid types - methane gas, water, and oil - in the microannuli: (i) from real cases and (ii) from the theoretical-based model (uniform microannuli). Furthermore, the second part investigates the fluid flow dynamics in uniform microannuli with different wall roughness, and it is a complement analysis of the experimental works investigating the effect of pipe surface roughness on the cement plug sealing. The overall simulation results suggest that the fluid flow phenomena in the actual microannuli depend on the microannuli morphology and the flowing fluid properties. Such microannuli with tortuous shape and low-connectivity potentially increase the resistance for fluid to flow.

Acknowledgment

Undertaking this Ph.D. has been a long journey for me, and it would be not possible without the support and assistance of all those who have been instrumental in the successful completion of this research study. First, I would like to express my deep gratitude to my supervisor, Sigbjørn Sangesland, for the opportunity given to me, for the guidance and positive encouragement he has given me during working on this research study.

I would also like to thank my co-supervisor, Torbjørn Vrålstad, the project manager from SINTEF for the guidance, planning the work, and the fruitful discussions. His professional attitude and constructive advice were helpful and improved my work during this research study.

I would like to thank the Research Council of Norway, Aker BP, ConocoPhillips, Equinor, and Wintershall for supporting and financing the work through the research center The Drilling and Well Centre for Improved Recovery (DrillWell). I appreciated the DrillWell center for organizing the research group and the annual meeting, which was a valuable platform for sharing and having a discussion with industry experts and diverse researchers.

I would like to acknowledge my colleagues from SINTEF, who have been very vital to this research work. I would like to thank Nils Opedal for the valuable guidance and assistance working on the experimental setup. I am also grateful for the time and efforts he put into helping and guiding me in solving the technical difficulties. I would also like to thank Ragnhild Skorpa, for introducing and guiding me with the fluid dynamic simulations and the valuable discussions, and I am also thankful for her advice on writing manuscripts. I want to thank the staff of SINTEF Laboratory for allowing me to conduct the hydraulic integrity test and all the technical supports.

I would like to express my gratitude to technical staff in NTNU Reservoir Laboratory and mechanical workshops for the help and supports during the permeability testing. I wish to thank friends and colleagues from the department who contributed greatly to my personal and professional time in Trondheim. Special thanks to Geir-Ove Strand, I Gusti Agung Gede Angga, and Titus N Ofei for the discussions and advice in writing this thesis.

Last but not least, my biggest thanks to my family and friends for the never-ending supports and encouragement during the study. I also wish to thank Steven for the patience and motivational supports and being my best friend.

"Every story starts with an idea, but it is the characters that move this idea forward."

— Michael Scott, The Alchemyst

Table of Contents

List of Publications

My contribution in terms of experimental/simulation work, analysis, and writing is stated in parenthesis:

- **Paper I,** "Laboratory Test on Cement Plug Integrity"
  Nils Opedal, Anisa Noor Corina, Torbjørn Vrålstad

  This paper was presented by Nils Opedal at ASME 2018 37th International Conference on Ocean, Offshore and Arctic Engineering in Madrid, June 2018 and published in the conference proceedings (40%, 20%, 10%).

- **Paper II,** "Cement Plug Sealing Studies of Silica Cement Systems"
  Anisa Noor Corina, Nils Opedal, Torbjørn Vrålstad, Sigbjørn Sangesland

  This paper was presented at ASME 2019 38th International Conference on Ocean, Offshore and Arctic Engineering in Glasgow, June 2019 and published in the conference proceedings (90%, 80%, 80%).

- **Paper III,** "The Effect of Casing Pipe Roughness on Cement Plug Integrity"
  Anisa Noor Corina, Nils Opedal, Torbjørn Vrålstad, Ragnhild Skorpa, Sigbjørn Sangesland

  This paper was accepted by SPE Drilling and Completion (95%, 80%, 80%).

- **Paper IV,** "Fluid Flow Analysis of Different Fluid Types Flowing Through Real Microannuli"
  Anisa Noor Corina, Ragnhild Skorpa, Sigbjørn Sangesland, Torbjørn Vrålstad

  This paper will be submitted for journal publication (90%, 80%, 80%).

ADDITIONAL PUBLICATIONS

- Strand, Geir-Ove and Corina, Anisa Noor. On Risk Control in The Well Plugging and Abandonment Phase: The Case of The Norwegian Continental Shelf. Journal of Petroleum Science and Engineering, Volume 183, December 2019.

CONFERENCES AND MEETINGS

- **Annual DrillWell Seminar.** Poster presentation: "Cement Plug Integrity in P&A Phase" on 27 September 2017, Stavanger, Norway.

- **Annual DrillWell Seminar.** Technical presentation: "The Effect of Casing Pipe Roughness on Cement Plug Integrity" on 26 September 2018, Stavanger, Norway.

- **SPE/IADC International Drilling Conference and Exhibition.** Technical presentation: "A Laboratory Study of the Effect of Casing Pipe Roughness on Cement Plug Integrity" on 7 March 2019, The Hague, Netherlands.

- **Annual DrillWell Seminar.** Technical presentation: "Fluid Flow Analysis of Different Fluid Types Flowing Through Real Microannuli" on 25 September 2019, Stavanger, Norway.

Nomenclature

Greek letters

μ	Fluid viscosity [Pa-s]
ρ	Fluid density [kg/m^3]
ΔP	Differential pressure [Pa, bar]
∇P	Pressure gradient [bar/m, kPa/m]

Roman letters

A	Coefficient describing energy losses due to the viscous effect
B	Coefficient describing energy losses due to the inertial effect
F_o	Forchheimer number
ID	Inner diameter, [cm, mm, inch]
K	Permeability, [Darcy]
L	Length [m]
OD	Outer diameter, [cm, mm, inch]
P	Pressure [bar]
P_I	Inlet pressure [Pa, bar]
P_S	Reference pressure at the standard condition [Pa]
Q	Volumetric flow rate [m^3/s, ml/min]
Q_{AV}	Average volumetric flow rate [m^3/s]
Ra	Surface roughness parameter based on the mean height [µm]
RS_m	Surface roughness parameter based on the spacing parameter [mm]
Rz	Surface roughness parameter based on the height discrimination [mm]
T	Temperature [T]
T_I	Inlet temperature [K, ^{o}C]
T_S	Reference temperature at the standard condition [K]

Abbreviations

BWOC	By weight of cement
C-S-H	Calcium silicate hydrate
CFD	Computational fluid dynamic
CT	Computed tomography
P&A	Plug and abandonment
STP	Standard temperature and pressure

Chapter 1
Introduction

1. 1 Background and motivation

Plug and abandonment (P&A) operation is not a new topic in the petroleum industry, and the practices have not changed much yet over time (NPC 2011, Khalifeh et al. 2019). Nonetheless, the subject has received a growing interest in the past years because many mature oil and gas fields are about to reach their end of productive life, and this signifies increased demands for P&A operation in the future (Trudel et al. 2019, Vrålstad et al. 2019). For example, in the Norwegian Continental Shelf, it was predicted that 12% of active wells (362 wells) would be decommissioned between 2016-2025 (Oil & Gas UK 2016). Furthermore, this growing interest in P&A has been intensified by the progressive change in the P&A regulations to include stricter requirements, driven by the increased awareness of environmental protection as a result of the 2010 Macondo oil spill in the Gulf of Mexico (Smith and Shu 2013, Vrålstad et al. 2019). Under these circumstances, the current attention is centered on developing optimal and cost-efficient strategies to achieve a long-lasting well abandonment.

One of the key parameters to achieve long-term integrity in the abandoned wells is the hydraulic isolation of the sealing material (Daccord et al. 2006, Oil & Gas UK 2015). Portland cement is one of the qualified sealing materials that is commonly used in the well abandonment. Good quality of set cement has the fundamental attributes for zonal isolation, as it retains a sufficient mechanical strength and has low porosity and permeability (Barclay et al. 2001, Nelson and Michaux 2006). But once the cement plug is placed downhole, it can be exposed and subjected to different loading scenarios that can be critical to the cement integrity, such as cement shrinkage, thermal and pressure variation from the surrounding formations and offset wells, or tectonic activities (Akgün and Daemen 1999, Mainguy et al. 2007, Bois et al. 2011, Therond et al. 2017, Bois et al. 2019). Defects in set cement can potentially develop into leakage pathways and increase the well effective permeability (Duguid et al. 2013, Gasda et al. 2013), and this condition can imply costly and difficult remedial plugging and safety issues. The raised concerns of cement integrity issues at the downhole underlines the need to seek more knowledge of the hydraulic isolation of the cement plug for well abandonment.

Relevant to the above scheme, laboratory tests of the isolating ability of a sealing material can be instrumental for analyzing the hydraulic integrity of a cement plug. The literature study shows that there were few numbers of experimental tests proposed to investigate the hydraulic

sealing of the cement plug, but the results were dispersed because the experimental setups were lacking consistency (Nagelhout et al. 2010, CSI Technologies 2011, Aas et al. 2016). Therefore, further evaluation of the hydraulic sealing performance of cement plugs is found necessary to carry out.

1. 2 Objectives

The main objective of this research work is to evaluate the hydraulic sealing performance of cement plugs inside pipes relevant for well abandonment. In order to assess the sealing performance of cement plug, a small-scale apparatus is built based on the design by van Eijden et al. (2017), which was also adopted in Oil and Gas UK guidelines (Oil & Gas UK 2015). Considering the novelty of the existing research on the function test, a preliminary study is conducted to investigate the functionality of the setup, generate baseline results, and establish the cement curing methods. The key findings from the preliminary study are then used as the reference for further experiments.

In the next step, comparative experiments are conducted to examine the effect of several influencing parameters on the cement plug isolation. In these experiments, the sealing performance of both neat cement and silica cement are tested and linked to parameters: (i) pipe surface roughness and (ii) curing temperature and expanding agent additive. Moreover, post-examinations on the cement plug samples, such as visual inspection and gas permeability measurements, are conducted to identify the location of the leak sources and analyze the possible mechanism failure.

Another objective of this research is to study the fluid flow dynamics in the cement defects of microannuli. A numerical simulation-based study of CFD is conducted, and the study is divided into two parts. The first part focuses on the investigation of fluid flow phenomena of three different fluids – methane gas, oil, and water – flowing in real microannuli and theoretical-based microannuli (uniform microannuli[1]). In the analysis, the fluid streamlines and flow regimes are characterized and associated with the microannuli morphology and the properties of flowing fluids. Furthermore, the analysis looks into the comparison in fluid dynamics between the real- and theoretical microannuli. The second part of the simulation study is a continuation of the experimental work investigating the effect of casing surface roughness on the cement plug sealing. In this part, the fluid flow dynamics in uniform

[1] The uniform microannuli is modeled to have a perfectly uniform aperture (or gap) with homogenous features at all sides.

microannuli with different wall roughness are investigated, and the results are used to analyze leak path characteristics in the tested cement samples.

The main contributions of the research work related to the above objectives are summarized in Fig. 1-1.

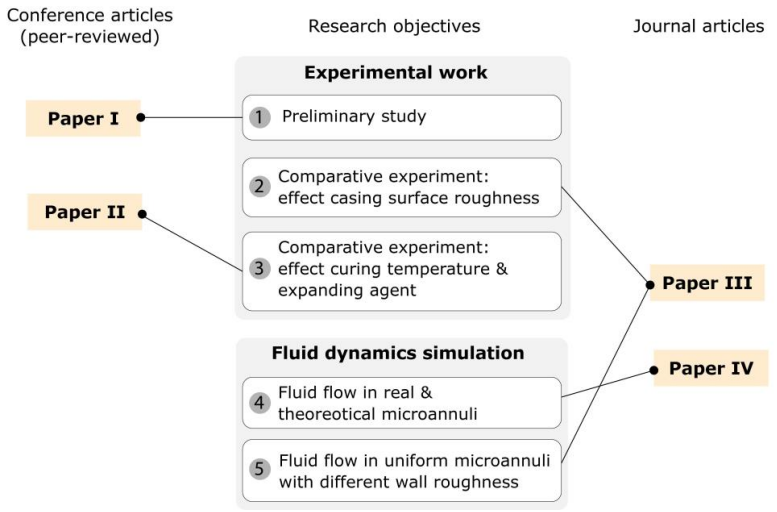

Fig. 1-1. The relationships between research objectives and research articles

1. 3 Thesis content

This Ph.D. thesis consists of this main report and four papers, enclosed in the Appendix. The main report includes the background and objectives of the study, the theoretical framework, and the summary of the main research work. An appendix is enclosed in the main report, providing additional information relevant to the main study. The detailed structure of this thesis is as follows:

- Chapter 1 outlines the background, motivation, and objectives of the research work.
- Chapter 2 presents the theoretical framework of cement plugs in the well abandonment relevant to the research work. It covers the overview of typical P&A operation, oilwell cement characteristics with few examples of special cement systems, and typical defects in set cement during the abandonment phases. The last part of this chapter describes the existing experimental setups for evaluating the hydraulic isolation of set cement.
- Chapter 3 describes the tools and procedures employed in the experimental part of this research. The first part describes the small-scale setup for the function test of cement

plug hydraulic sealing. The last part of this chapter describes the gas permeameter and the surface roughness measurement tool.

- Chapter 4 presents the experimental work of this research study. The first part presents the preliminary study on the setup for the function test (Paper I). The remaining parts present the comparative experimental tests of the cement plug sealing performance with different investigated parameters: (i) casing pipe roughness and cement systems (Paper III) and (ii) curing temperature and expanding agent additive (Paper II). In each part, the materials and setups are described, and followed by results and discussion.
- Chapter 5 presents the simulation work investigating the fluid dynamics of flow through microannuli. The first- and second parts of the simulation work are discussed consecutively in this chapter.
- Chapter 6 presents the conclusions from the findings and analysis in the research work and recommendations for future study.

Chapter 2
Cement plug for well plugging and abandonment

2. 1 Overview of P&A operation

The life-cycle of a well begins when it is spudded and ends when it is permanently abandoned. During this life-cycle, a well can enter one or several states, and eventually, it will be permanently abandoned after fulfilling its purpose (Kaiser 2017). In many regions, well abandonment operations must strictly comply with the abandonment regulations and standard guidelines issued by the government authorities in place or the industry associations. Although the requirements could vary, the intent of the P&A operation essentially is to achieve the permanent isolation of the penetrated formations, preventing fluid migration to the surface, freshwater, and surrounding formation (Liversidge et al. 2006, Abshire et al. 2012).

The details of P&A operations could differ depending on the well characteristics, and typically it requires the removal of completion or production hardware and installation of the necessary sealing materials. Based on the standard in the Norwegian sector, NORSOK D-010, permanently plugged wells require two independent permanent well barriers placed at the level of the reservoir/perforation and the potential flow zones in the overburden, and one permanent well barrier installed at the shallow level or below the surface bed, as illustrated in Fig. 2-1 (NORSOK 2013). It is also stated that the permanent well barrier shall extend the full cross-section of a wellbore, from formation to formation, including the annuli, preventing fluid flow in the lateral and vertical direction.

There are various sealing materials that can be used for plugging wells, and these materials must fulfill the required criteria to effectively and successfully plug the well. The requirements are as follows (NORSOK 2013):

- provide long-term integrity
- impermeable;
- non-shrinking;
- able to withstand mechanical loads;
- chemically resistant;
- ensure bonding to steel;
- not harmful to the steel tubular integrity.

Portland cement has been used as a plugging material in the oil fields around 1920s (King and Valencia 2014), and it is the most common material used because it is widely available and fulfills the essential criteria of hydraulic sealing, e.g., impermeable (Nelson and Michaux 2006). Alternative and emerging plugging materials may also be used for P&A operation, such as blast furnace slag, bentonite, low melting point metal alloys, resins, formation, and thermite (Khalifeh et al. 2013, Oil & Gas UK 2015, Vrålstad et al. 2019).

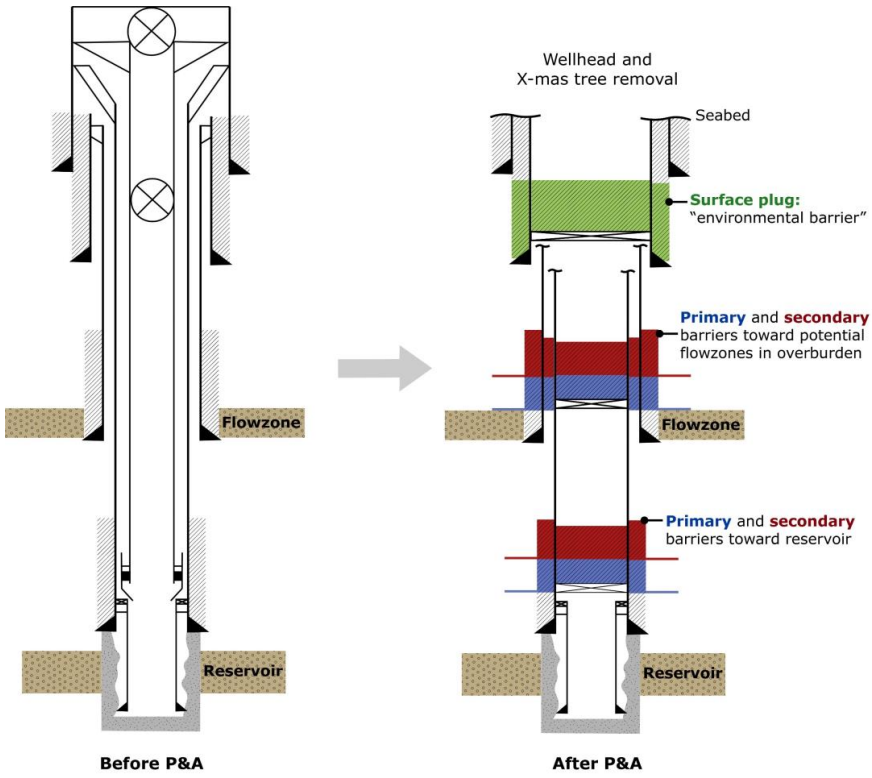

Fig. 2-1. A simplified illustration of a typical offshore well before and after abandonment, adapted from Vrålstad et al. (2019). The color-coding of the barrier was based on the definitions from NORSOK (2013).

2. 2 Portland cement and special cement systems

Portland cement is commonly manufactured for the use in oil well cementing. Based on the manufacture and cement composition, oilwell cement is classified into eight classes of API-ISO cement (Nelson and Michaux 2006). Among those, the class G well cement is the most commonly used, and it is intended for use as a basic well cement. Primarily, the Portland cement clinker consists of hydraulic calcium silicates, calcium aluminates, and calcium aluminoferrites.

The cement clinker phases are anhydrous and chemically react with water when they are in contact, forming solid hydrated products. The predominant phase of the hydrated products is quasi-amorphous calcium silicate hydrate (C-S-H), which constitutes roughly 65% of fully Portland cement at ambient conditions. Another cement hydration product is calcium hydroxide (Portlandite), which is highly crystalline and fills around 15%-20% (Powers 1958, Nelson and Michaux 2006). As hydration continues, more products occupy the spaces between and among the cement grain, forming a dense microstructure that adds sufficient strength to the cement. The hydrated cement intrinsically has low porosity and permeability (Powers 1958).

The chemical reaction during the hydration process leads cement to shrink because the volume of the product is less than that of the reactant, and this process is usually known as chemical shrinkage. The amount of chemical shrinkage is approximately 6.4 ml/100 g cement reacted (Powers 1958). Before the skeleton of hydration products develops, cement can deform freely from this shrinkage. And after the skeleton is formed, the chemical shrinkage becomes restrained due to the rigid structure of cement, and it can occur as autogenous shrinkage. The autogenous shrinkage is the external volume reduction caused by the mechanical response to capillary stress generated by chemical shrinkage, ranging from 0.5-5% volume reduction (Thiercelin 2006). This degree of shrinkage is highly dependent on the curing condition (water-to-cement ratio, temperature, and pressure), cement clinker properties, and additives (Reddy et al. 2009). The cement shrinkage becomes one of the challenges in well cementing because the volumetric reduction can induce cracks or microannuli (Bois et al. 2011).

In some instances, an expanding agent can be added into the cement to counteract the shrinkage, and several studies have linked the positive performance of the expanding agent to reduce the risk of crack or debonding (Boukhelifa et al. 2004, Nagelhout et al. 2010, Aas et al. 2016). In general, the cement expansion can be achieved through mechanisms of (i) crystal growth or (ii) gas generation (Nelson et al. 2006). One of the examples of the former mechanism is the use of calcined magnesium oxide that can induce an expansive force, which is exerted from the hydration of magnesium oxide to produce an oxide mineral (or a crystal of magnesium hydroxide). This expansive force could displace the cement components and increase the bulk volume of the cement matrix (Ghofrani and Plack 1993).

Other types of special cement systems are typically used to address particular wellbore problems, for example, high-temperature wells. The biggest challenge of a wellbore with high downhole temperature is the significant deterioration of the physical and chemical behavior of neat well cement. At an elevated temperature higher than 110^{o} C, the C-S-H phase often

converts to alpha dicalcium silicate hydrate, a highly crystalline phase that is very weak and porous (Eilers and Root 1976, Nelson and Barlet-Gouédard 2006). This metamorphism ultimately could both decrease the compressive strength and increase the permeability of the set cement, also known as strength retrogression. One of the solutions to prevent this event is the addition of silica, such as silica flour or silica fume, into the cement system to promote the formation of C-S-H phase through the chemical reaction between silica and calcium hydroxide, also known as pozzolan reaction (Patchen 1960, Grabowski and Gillott 1989, Gaurina-Međimurec et al. 2017).

2. 3 Potential leakage pathway and failure mechanism of set cement in P&A wells

The integrity of permanently abandoned wells could be compromised if damages present in the wellbore barriers, potentially contribute to the evolution of leakage pathways. In both cement plug and cement sheath, leakage could occur through defects formed in the body of the set cement, for example, set cement with low permeability and porosity or cracks/voids (Fig. 2-2). It could also occur through pathways formed around the cement body, from channeling or debonding at the interface between cement/casing or cement/formation.

These cement damages could be induced by different mechanisms that arise during or after plugging operation, and the following mechanisms were suggested as the main reason (Trudel et al. 2019) :

- *The time-dependent deformation* mechanism involves the cement shrinkage during the initial hydration process, which could risk diminishing the cement integrity through the formation of shrinkage cracking or microannulus. The cement hydration progressed for an extended period, but at a later age, the process is diffusion-driven at a slow rate.
- *Chemical degradation* typically occurs due to the presence of reactive fluids in the wellbore, such as H_2S, CO_2, or brine, that could induce chemical reaction with the basic compounds in cement and deteriorate the cement properties.
- *Pressure and thermal stress variation* during the abandonment phase could arise from the operations on the neighboring wells, such as active steam or water injection, hydraulic fracturing, or tectonic activity. Numerical studies found that stress variations could induce mechanical failure in the set cement (Akgün and Daemen 1999, Mainguy et al. 2007, Bois et al. 2011, Bois et al. 2019).

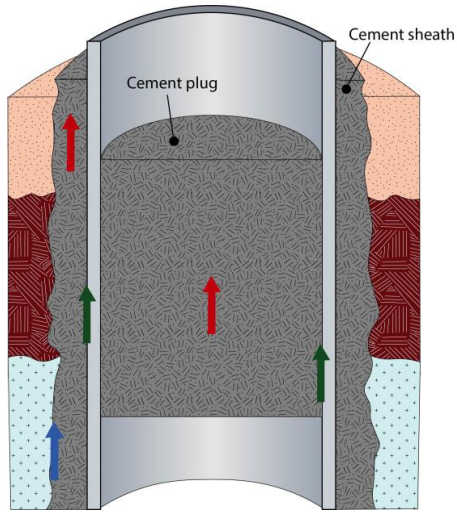

Fig. 2-2. The possible leakage pathways in cement plug and sheath: (a) red arrow: flow through the cement body, (b) green arrow: flow through the pathway formed at the interface between casing/cement, and (c) blue arrow: flow through the pathway formed at the interface between formation/cement. The figure was adapted from Vrålstad et al. (2019)

In addition to the above mechanisms, Kiran et al. (2017) implied that failure in cement integrity could be attributed to the in-situ or physical factors, often related to the operational procedure (e.g., cement placement) and the use of materials. Others suggested that factors such as the completion type, well vintage, and regulatory guidelines also play a particular role in the well integrity (King and Valencia 2014, Kaiser 2017). Nevertheless, the root of failures in the well abandonment may be difficult to diagnose or observe, and they are likely impacted by multiple mechanisms.

2. 4 Existing experimental tests of cement hydraulic integrity

The assessment of the hydraulic isolation of set cement requires a purpose-built setup with fluid flow rate measurement as a leakage indicator. The studies investigating the sealing ability of a set cement have been ongoing since the 1960s, and most of the early studies focused on the importance of effective bonding at the interface of cement/casing or cement/rock to provide adequate protection against leakage (Evans and Carter 1962). The required bonding strength at the interface to prevent fluid from flowing is defined as the hydraulic bond strength (Opedal et al. 2019). Several studies have measured and correlated the hydraulic bonding strength of cement with several parameters, such as cement types and additives, casing coating and materials, formation types, wetting fluid types, and mud removal (Evans and Carter 1962, Carter and Evans 1964, Scott and Brace 1966, Khalifeh et al. 2018). Although these studies provided beneficial insight of the interaction between cement slurry and casing/formation to

form initial bonding, bonding was no longer assumed as the only parameter that contributes to leaking cement (Bois et al. 2011).

Further experimental studies started to look into the effect of mechanical and thermal loads, which could arise from different downhole operations, on the cement sealing performance. The operating conditions simulated in these studies include pressure test (Goodwin and Crook 1992), thermal and pressure cycling (Jackson and Murphey 1993), and water injection (Therond et al. 2017). Aside from the hydraulic sealing assessment, these studies also examined the type of failure mechanism induced by the applied loads. The overall findings of these studies deliver comprehensive information of cement hydraulic sealing under different cases of realistic operating condition, but the results were only relevant to the annular sealing of the cement sheath.

Relevant to the internal casing isolation for well abandonment, a specific laboratory setup to test the hydraulic sealing of the cement plug is required, and there were few existing studies conducted the analysis (Nagelhout et al. 2010, CSI Technologies 2011, Aas et al. 2016). In these studies, the test was performed by measuring the water/gas leak rate through plug material placed in the casing pipe, subjected to differential pressure. However, to produce comparable results, the experimental assessment should be run by using a consistent apparatus and testing protocol (Nagelhout et al. 2010). Following these studies, van Eijden et al. (2017) proposed the design of small- and large-scale experimental equipment for a functional test of a full-bore plug that has a similar test principle to former setups. It has an additional feature that allows uninterrupted cement curing and testing processes in a controlled environment to simulate the realistic downhole condition. The design of this experimental setup was also included in Oil and Gas UK guidelines as a function test for sealing material qualification (Oil & Gas UK 2015).

Chapter 3

Methods of the experimental works

This chapter presents the tools used for the experimental works, which include (i) the cement-plug hydraulic integrity setup, (ii) gas permeameter, and (iii) surface roughness measurement tool. The details of the procedure and outputs from the measurement are also included for each described tool.

3. 1 Function test of the cement plug hydraulic sealing

A small-scale laboratory setup was built and used to evaluate the sealing ability of the cement plug, as seen in Fig. 3-1. The setup was constructed based on the function test proposed by van Eijden et al. (2017) and had the following design features:

- Curing and testing the cement plug at elevated pressure and temperature to approximate the actual downhole condition.
- The adjustable platform system installed in the setup allows uninterrupted curing and testing processes consecutively to minimize changes in cement and casing properties.
- The setup is connected to an automatic system, and thus the test can be conducted with minimized effects of human factors.
- The test procedure when creating the differential pressure across the cement plug is designed to avoid ballooning of the test cell.
- The test outputs are used to indicate the minimum pressure required for gas to flow (breakthrough pressure) and the gas leak rate if the cement plug fails to seal.

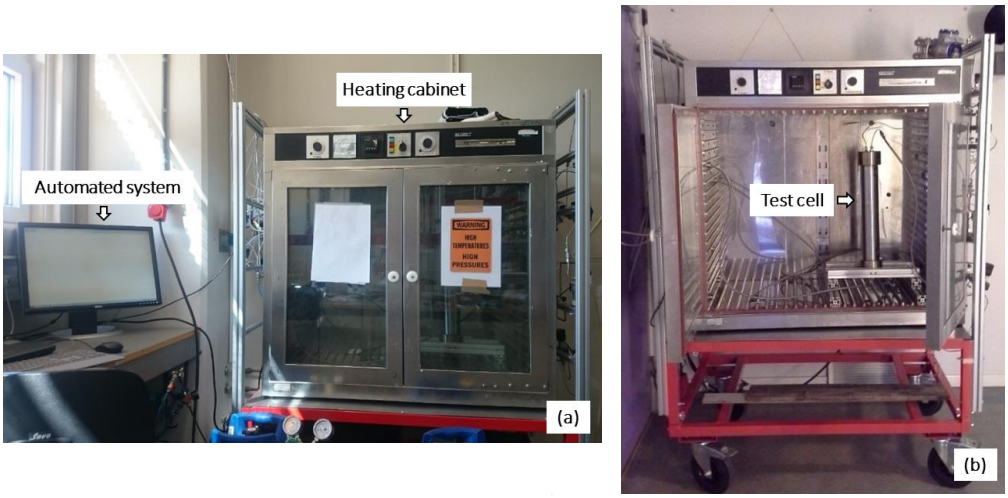

Fig. 3-1. The small-scale laboratory setup for testing cement plug integrity

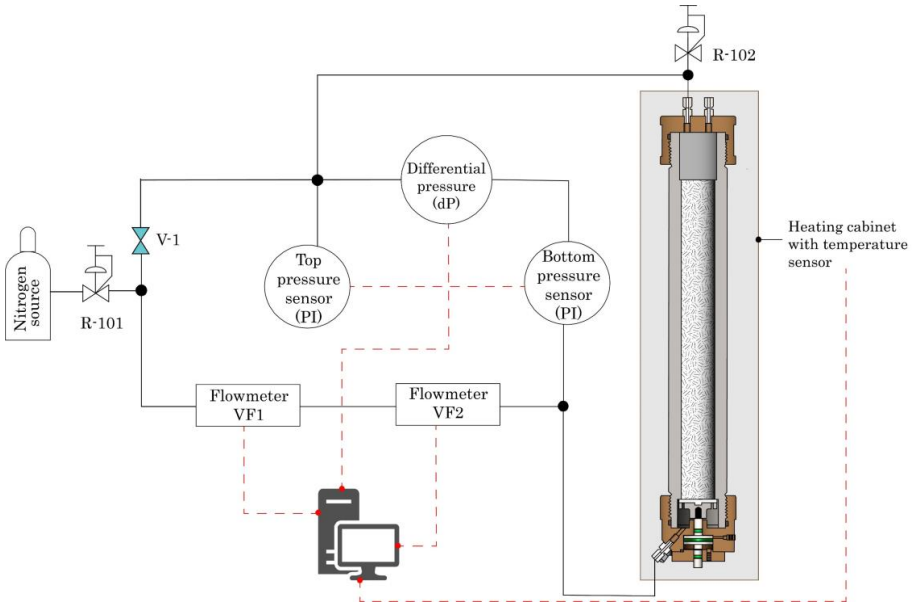

Fig. 3-2. The simplified layout of the function-test setup with the essential elements

3.1.1 Setup components and test cell

Fig. 3-2 shows the layout of the key components composing the experimental setup, which functions are explained as follows:

- A test cell to simulate the cement plug inside a pipe, and it is placed inside a heating cabinet.
- A heating cabinet to heat the test cell, equipped with a temperature sensor and a controller.
- A nitrogen source to pressurize the test cell.
- A manual pressure regulator (R-101) to manually control the pressure within the system.
- Two Bronkhorst Mass Flow Meters (VF1 and VF2) to measure the gas flow rate. The flowmeter VF1 measures up to 56.25 ml/min, and VF2 measures up to 562.5 ml/min. Both flow meters measure the mass flow rate of gas at the standard condition of pressure 1 bar and temperature of 20^{o} C.
- Two GE-Druck pressure indicators (PI), each connected to the top and bottom side of the test cell, to detect pressure change in the system.
- One Fuji Electric FCX pressure transmitter (dP)[1] to measure the differential pressure between the pressure indicators.

[1] The pressure transmitter has the smallest resolution of 0.01 bar

- An automated pressure regulator (R-102)[1] to automatically control the pressure inside the system.
- A data acquisition system to read and record measurements from different sensors periodically (usually per 10 seconds). It also can control the adjustable platform system inside the test cell.

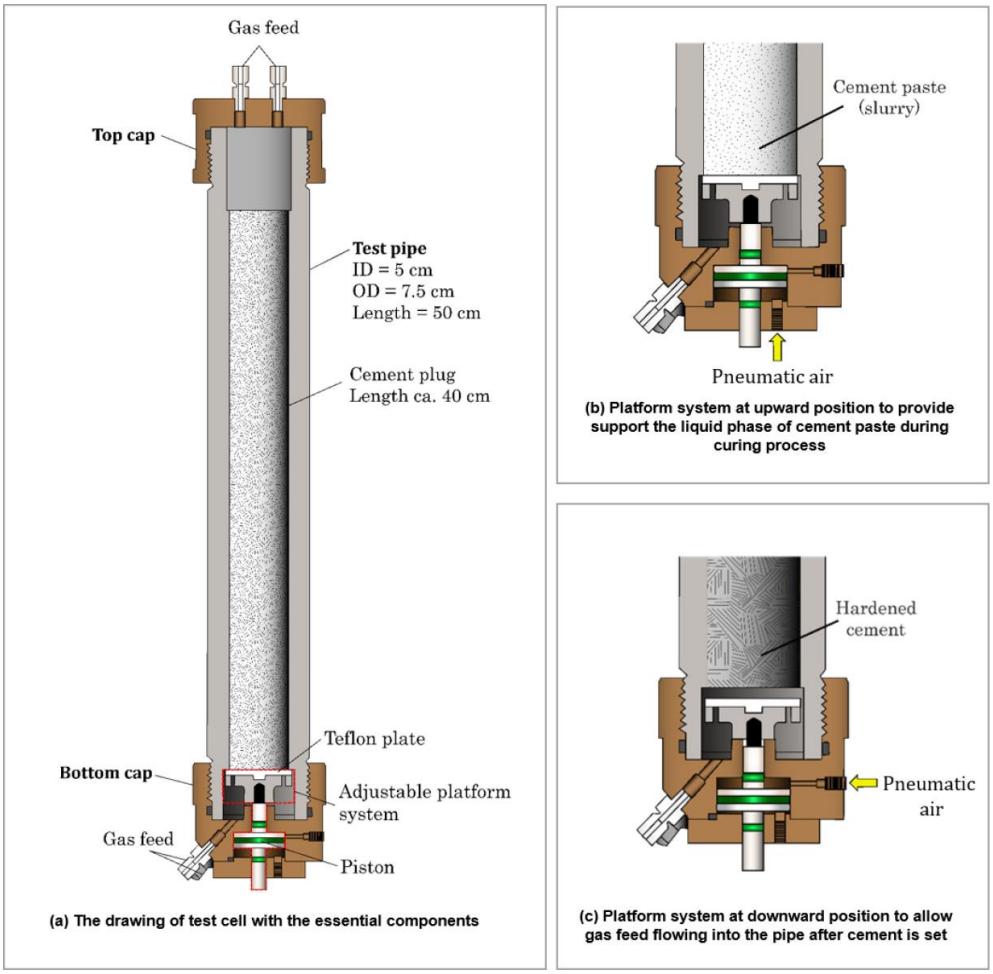

Fig. 3-3. The schematic drawing of the test cell

Fig. 3-3 shows the details of the test cell. The test cell has three main parts, described as follow:

1. A steel pipe (or casing). It is used to contain a cement column and has a dimension of the outer diameter (*OD*) of 7.5 cm (3”), the inner diameter (*ID*) of 5 cm (2”), and a height of 50 cm (19.6”).

[1] The pressure regulator has the smallest resolution of 0.01 bar.

2. Top cap, with Swagelok 1/8” connection ports. It can be screwed to the top side of the pipe, and the port allows pressurized gas to flow into the pipe.
3. Bottom cap, with Swagelok 1/8” connection ports. It has a similar property and function with the top cap. In addition to that, the bottom cap contains an adjustable platform system. The platform consists of a Teflon plate and mounted to a vertically moving piston, which is connected to a pneumatic system to move the piston up and down. When the platform is in an upward position, it supports the cement slurry inside the test cell. After the cement is cured and ready to be tested, the platform is switched downward. The Teflon plate is used to avoid cement to stick.

The empty test cell has been tested to the high pressure of 100 bar, and there were no signs of pipe deformation or damages on the pipe threads.

3.1.2 Test preparations and procedure

There are two preparation processes before the hydraulic integrity test is conducted. The overall processes are explained in sequence as follow:

Pressure test before cement curing

Before every experiment, a pressure test is conducted to examine leaks inside the connection tubing and the test cell. First, the empty test cell is mounted to the pressure board. Then, the system is pressurized to the working pressure of 20 bar by opening the nitrogen feed and closing the valve R-102. After the pressure in the system stabilizes, the nitrogen feed is closed, and the pressure is monitored. As an ideal state, the setup must hold constant pressure for 1 hour.

Preparation for curing cement plug

Before placing the cement in the pipe, the test cell is preheated to the test temperature, and the platform system is switched to an upward position. Afterward, the cement slurry is poured by gravity into the pipe, and the top cap is screwed tightly to the pipe. Then, the system pressure is increased to the curing pressure at a slow rate, and the test cell is left for curing in the heating cabinet for four days.

Cement integrity test

1. Shift the adjustable platform system in a downward position.
2. Close valve V-1 (see Fig. 3-2) to create a by-pass line through the test cell. Consequently, there would be two pressure lines, going to each side of the test cell, which can be regulated separately. The pressure on the bottom side is regulated by the regulator R-101, while the pressure on the top side is regulated by the regulator R-102.

3. Decrease the pressure on the top side to create a pressure drop across the cement plug. Wait until the pressure is stabilized.
4. Monitor the flow rate. If a leak is detected, keep monitoring the flow rate until the flow rate stabilized or reached a steady-state condition.
5. Repeat steps 3-4 and further reduce the top pressure to generate a higher differential pressure. The test is stopped when one of the test conditions below is reached:
    - The flowmeter VF2 reached the maximum reading.
    - The top pressure reached atmospheric pressure.

3.1.3 Test output

The typical reading of flow rate and differential pressure during the test is shown in Fig. 3-4. For data analysis, the flow rate reading must be corrected if elevated pressure and temperature were applied in the test. This process is required because the flowmeters measure the mass rate of nitrogen gas at the standard condition, and they are not sensitive to change in pressure and temperature within the setup. The corrected volumetric flow rate of nitrogen flowing through the cement plug, Q, is calculated as follows:

$$Q = Q_{STP} \cdot \frac{P_s}{P_I} \cdot \frac{T}{T_s} \quad \text{(Eq. 3-1)}$$

where Q_{STP} is the flow rate of nitrogen measured by the flowmeter at standard temperature and pressure, or STP (m^3/s), P_S is the reference pressure at STP ($1x10^5$ Pa), P_I is the inlet pressure (Pa), T is the test temperature (Kelvin), and T_S is the reference temperature (293.15 K). After corrected, the test output can be used to generate the following information:

- the required differential pressure for gas to flow through cement plug for the first time (breakthrough pressure), and
- the relationship between pressure gradient (∇P) and flow rate (Q), shown in Fig. 3-5, which is practical for comparing the results of several samples.

3. 2 Gas permeability measurement

A gas permeameter was used to measure the gas permeability of the cement plug samples. The tool was provided by Top Industrie and equipped with a Hassler test cell. Prior measurement, the cement plug sample was drilled to take out the core samples with a diameter of 3.86 cm (1.5”) and a length of 4 ± 1 cm. After the samples are dried in the oven at T= 60° C for 48 hours, the gas permeabilities were measured and averaged.

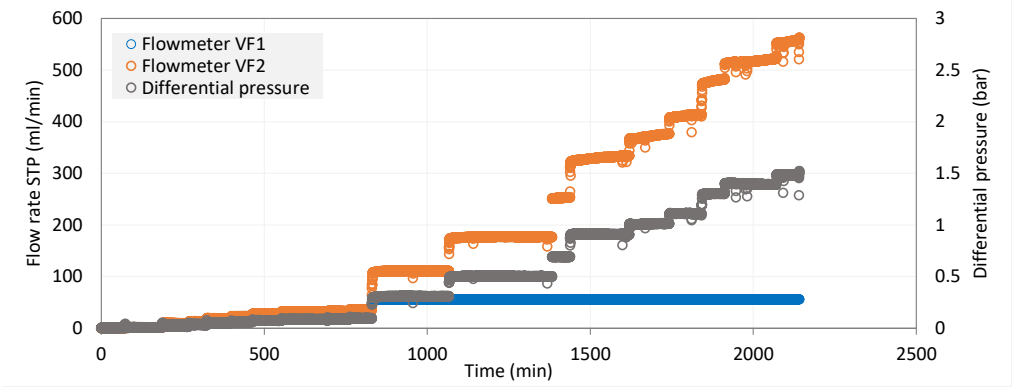

Fig. 3-4. Example of output from cement integrity test, showing flow rate at STP and differential pressure as a function of time of the test

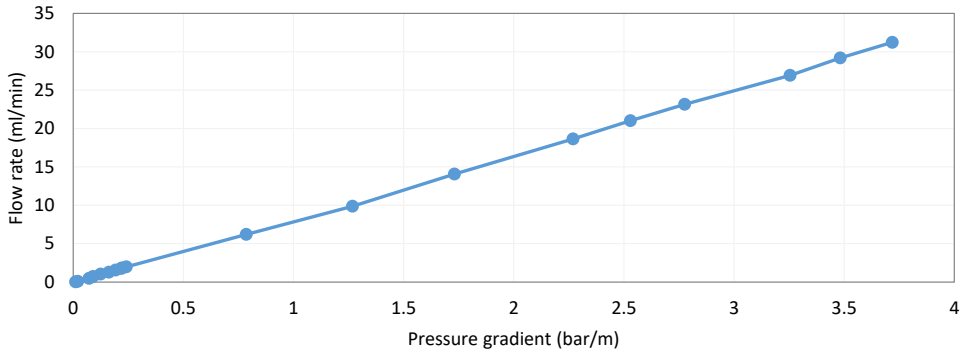

Fig. 3-5. Example of the plot of ∇P vs. Q (flowmeter VF2) from the output in Fig. 3-4

The fluid flow rate can be calculated from the permeability value, assuming laminar, single-phase, and linear Darcy flow, following the equation below:

$$Q_{AV} = \frac{KA}{1.013 \times 10^{12}\,\mu} \cdot \frac{\Delta P}{L} \qquad \text{(Eq. 3-2)}$$

where Q_{AV} is the average volumetric flow rate of nitrogen at the average pressure and temperature during testing (m^3/s), K is the gas permeability (Darcy), ΔP is the differential pressure across the specimen (Pa), L is the length of specimen (m), A is the cross-sectional area of specimen (m^2), μ is the nitrogen viscosity at the test temperature[1] (Pa-s).

3. 3 Surface roughness measurement

The surface roughness measurement tool used in this study was MarSurf PS 10, and it was equipped with a removable drive unit containing a stylus with a radius of 2 µm (Fig. 3-6). This

[1] The nitrogen viscosity is approximately 19.895 x 10^{-6} Pa-s at P=20 bar and T=66° C, and 22.128 x 10^{-6} Pa-s at P=20 bar and T=120° C

stylus is the active contact between the instrument and the surface, taking traces the profile of a surface. The collected traces then translated into a value of surface roughness and visualized in a graph. In this study, the tool was used to obtain the surface profile on the inner side of the test pipes. For each pipe, the roughness was measured at five different points along the pipe circumference to check the surface uniformity, and then the measurements were averaged.

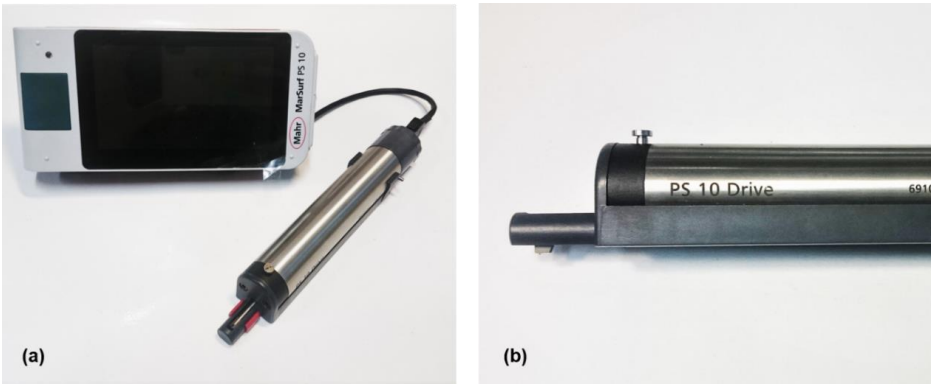

Fig. 3-6. Surface roughness measurement tool: (a) MarSurf PS10, with (b) a removable drive unit and stylus probe

There are three different roughness parameters relevant for this study; (i) Rz, (ii) RSm, and (iii) Ra. Each roughness parameter measures different characteristics of the pipe surface profile, and hence the use of these parameters will depend on the context of the investigation. The details of these roughness parameters are explained as follow:

i. Rz, a parameter of height discrimination of the profile element, as illustrated in Fig. 3-7. It measures the arithmetic mean value of the vertical distance from the highest point of peak profile to the adjacent lowest point of valley profile within a sampling length, as described by the following equation:

$$Rz = \frac{Rz_1 + Rz_2 + Rz_3 + \ldots + Rz_n}{n} \quad \text{(Eq. 3-3)}$$

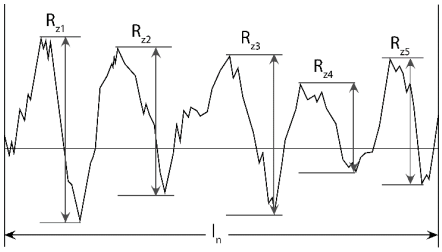

Fig. 3-7. Illustration of *Rz* measurement on a profile element

ii. RSm, a spacing parameter for describing the surface profile of an element with a periodic interval, i.e. a structure that repeats in a particular frequency, as illustrated in Fig. 3-8. It

measures the averaged value of the length along the mean line section that includes a peak profile and an adjacent valley, as described by the following equation:

$$RSm = \frac{RS_1 + RS_2 + RS_3 + \ldots + RS_n}{n} \quad \text{(Eq. 3-4)}$$

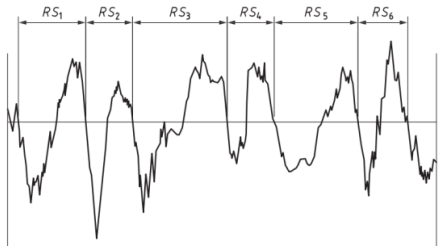

Fig. 3-8. Illustration of *RSm* measurement on a profile element

iii. Ra, a roughness average that measures the mean height of an element profile, as illustrated in Fig. 3-9. It is the average value of the absolute height of the profile from the reference line throughout the sampling length, as described by the following equation:

$$Ra = \frac{|z_1| + |z_2| + |z_3| + \ldots + |z_n|}{n} \quad \text{(Eq. 3-5)}$$

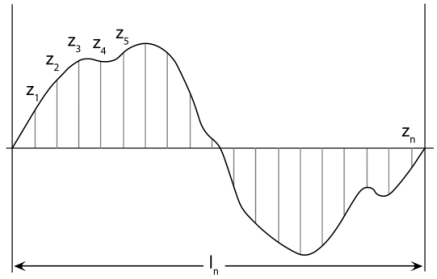

Fig. 3-9. Illustration of *Ra* measurement on a profile element

Chapter 4

Experimental results of cement plug sealing

The following chapter presents the preliminary study of the function-test apparatus and the comparative experimental tests investigating the cement plug sealing performance with different investigated parameters. The details of test material, results, and discussions are provided in each investigation.

4. 1 The preliminary study of the function test (Paper I)

The preliminary experiment was conducted to provide an initial understanding of the setup functionality and define the testing protocol. This step was also essential for establishing the baseline result as a basis for the analysis of future experiments. In this preliminary test, two different curing processes were investigated, with the description as follow:

1. Dry-cured test. The specimens in this test were cured in a sealed condition – i.e. no access to external water (Fig. 4-1a). The length of the cement plug was ~40 cm.
2. Wet-cured test. The specimens in this test were cured with an additional water column placed at the top of the cement slurry (Fig. 4-1b). Otherwise stated, the length of the cement plug was ~40 cm, with a ~4 cm water column.

4.1.1 Materials

The cement system chosen for the baseline test was a neat cement system, which was a mixture of Portland cement Class-G (NORCEM AS) and water without any additives. The cement was mixed following the guidelines in API RP 10B. The test cell pipes for the current test were smooth surface pipes (Ra~ 2-5 μm) without any surface coating. Samples for both tests were cured at a temperature of 66^{o} C and pressure of 20 bar.

4.1.2 Results and discussion

The ∇P vs. Q plot of three parallel dry-cured samples is shown in Fig. 4-2. All samples produced approximately linear curves that extended adjacently, indicating good repetitions and reproducibility. The breakthrough pressure in all samples could not be observed because immediate leak occurred at a significantly low differential pressure (<0.01 bar) just after the test was initiated.

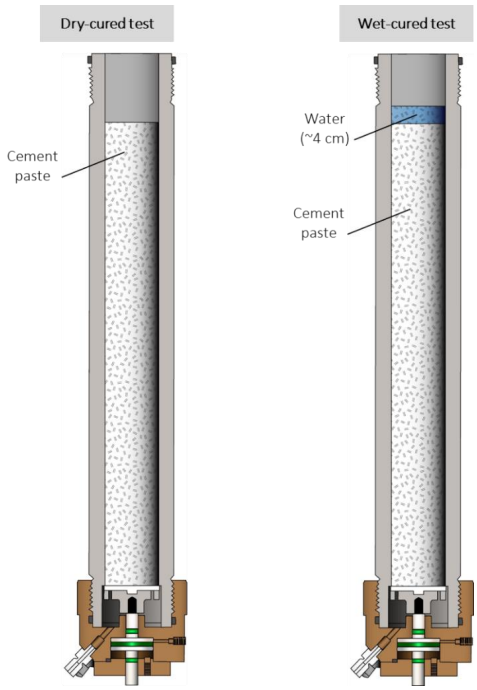

Fig. 4-1. Illustration of dry-cured and wet-cured test

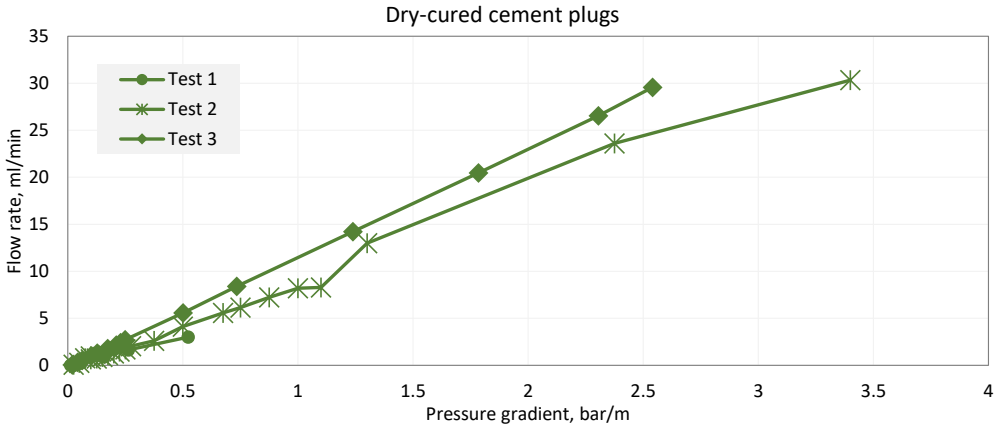

Fig. 4-2. Results of dry-cured samples presented in ∇P vs. Q plot

Opposite of the result from dry-cured samples, high breakthrough pressure, ~10 bar, was observed in the three parallel wet-cured samples, as shown by the example in Fig. 4-3 and the summary in Table 4-1. This event could be attributed to the reduced volumetric shrinkage from adding water on top of the cement slurry. The wet-curing process might also promote capillary effect, so additional pressure might be required for gas to displace water trapped in the cement pore. Furthermore, the wet-cured samples produced relatively low leak rates. The wet-curing method might be relevant to the downhole condition, where additional water sources are

present and can be accessed by the cement. However, the experimental results show variability of leak rate at the same differential pressure between each sample (Table 4-1). Because other information was limited to obtain, for example, the flow paths inside the cement plug, it was difficult to compare the flow rates from the wet-cured samples.

Overall, findings from the preliminary study showed that the function-test setup for evaluating the cement plug sealing was operational. Furthermore, the baseline results were established based on dry-cured Portland cement Class-G with no additives. The dry-cured method was implemented for future tests in this research work because the dry-cured samples were found to give reproducible results of both breakthrough pressure and flow rates.

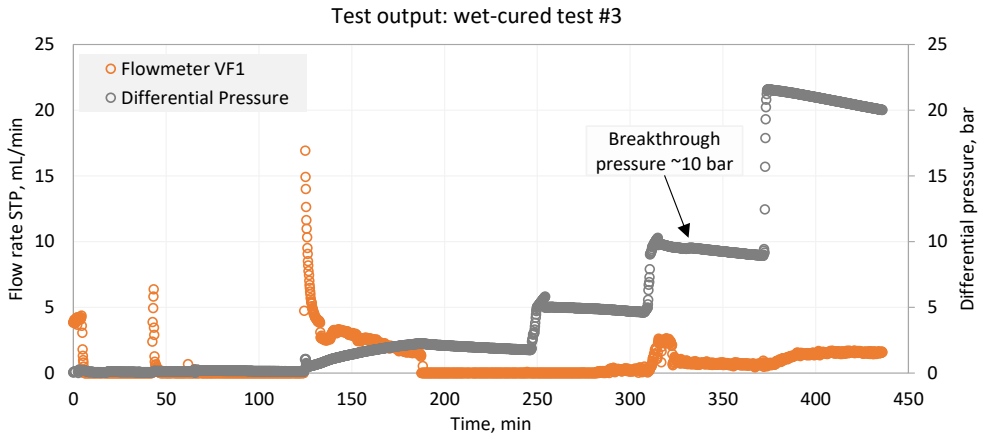

Fig. 4-3. The example of the results of a wet-cured sample from Test 3

Table 4-1. The summary of the breakthrough pressure and flow rate at ΔP=20 bar from wet-cured tests

Wet-cured samples	Breakthrough pressure (bar)	Flow rate at ΔP=20 bar (ml/min)
Test 1†)	10	3
Test 2	10	0.008
Test 3	10	0.09

†) The length of the cement slurry and water column was respectively 26 cm and 13 cm

4. 2 Effect of casing surface roughness on neat and silica cement systems (Paper III)

4.2.1 Materials

Test cell pipes

The test cell pipes were prepared with no coating and had three different inner surface roughness, and they were categorized as smooth, moderate-rough, and high-rough pipes, as seen in Fig. 4-4. The inner surface of moderate- and high-rough pipes was milled by using an indented grooving insert, and hence, it had a profile of a repetitive peak-valley cycle, as shown in Fig. 4-5. The measured roughness of these pipes is summarized in Table 4-2. The main

difference between the two rough pipes was located on the *Rz* value and the valley depth, see Table 4-2 and Fig. 4-5.

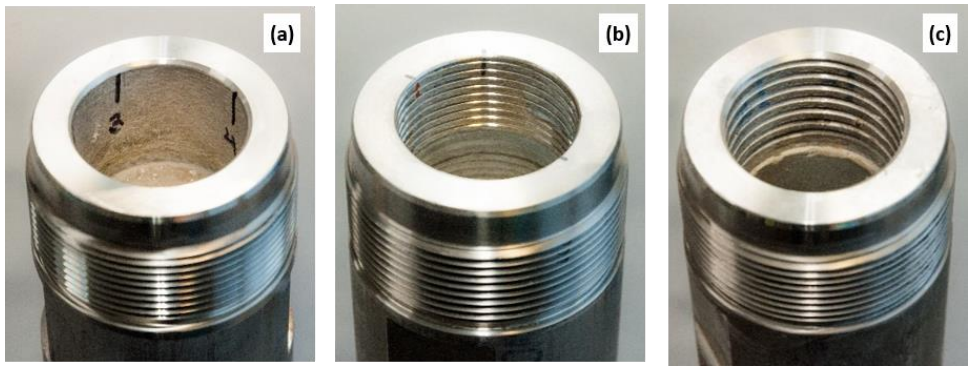

Fig. 4-4. Pipes with different inner surface roughness: (a) smooth-, (b) moderate rough-, and (c) high-rough pipes

Table 4-2. The averaged spacing and height parameters for all types of pipes

Pipe type	*Rz* (mm)	*RSm* (mm)	Valley width‡) (mm)	Peak width‡) (mm)
Smooth	0.042	1.118	N/A	N/A
Moderate roughness	1†)	2.962	1.074	1.934
High roughness	2†)	4.906	2.657	1.929

†) *Rz* value of the rough pipes ≈ the grooving depth
‡) *RSm* ≈ valley width + peak width

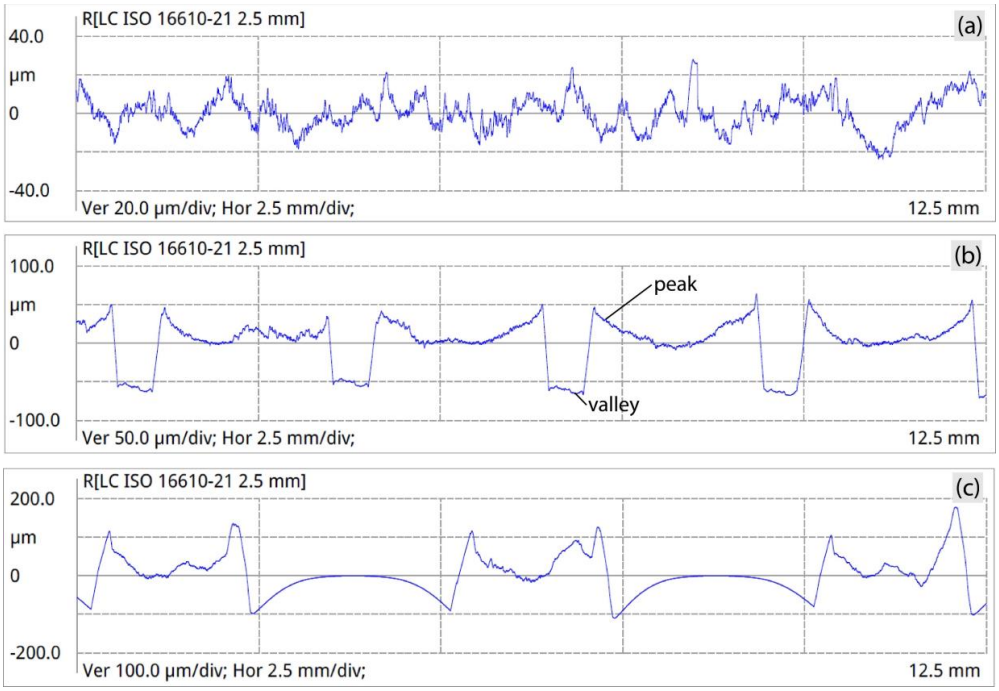

Fig. 4-5. Example of the surface profile of (a) smooth-, (b) moderate rough-, and (c) high rough pipes measured by using MarSurf PS10. The x-axis shows the sampling length of 12.5 mm, whereas the y-axis shows the roughness.

Cement systems

Two different cement systems were investigated: (i) neat- and (ii) silica cement system. The cement grain was Portland cement Class-G (NORCEM AS), and the form of silica used for silica cement was silica flour. The mix design of both systems is summarized in Table 4-3, and they were mixed following the guideline of API RP 10B. After the slurry was placed in the test cell, the samples were dry-cured for four days at a pressure of 20 bar. Samples of neat cement were cured at a temperature of 66° C, whereas samples of silica cement were cured at a temperature of 120° C.

Table 4-3. Mix design of the neat- and silica cement systems

Cement type	Water (% water-to-cement ratio)	Silica flour (% by weight of cement, BWOC)
Neat cement	44	-
Silica cement	62	35

4.2.2 Results and discussion

Based on the cement and pipe configuration, five test cases were conducted (Table 4-4), and three parallel samples were tested for each case. Results of neat- and silica cement plugs placed in different pipe roughness are shown respectively in Fig. 4-6 and Fig. 4-7.

Table 4-4. The experimental cases based on the evaluated parameters

Cement type	Pipe type		
	Smooth	Moderate roughness	High roughness
Neat cement	v[†)]	v	v
Silica cement	v	-	v

[†)] This was the baseline results from the preliminary study (Paper I)

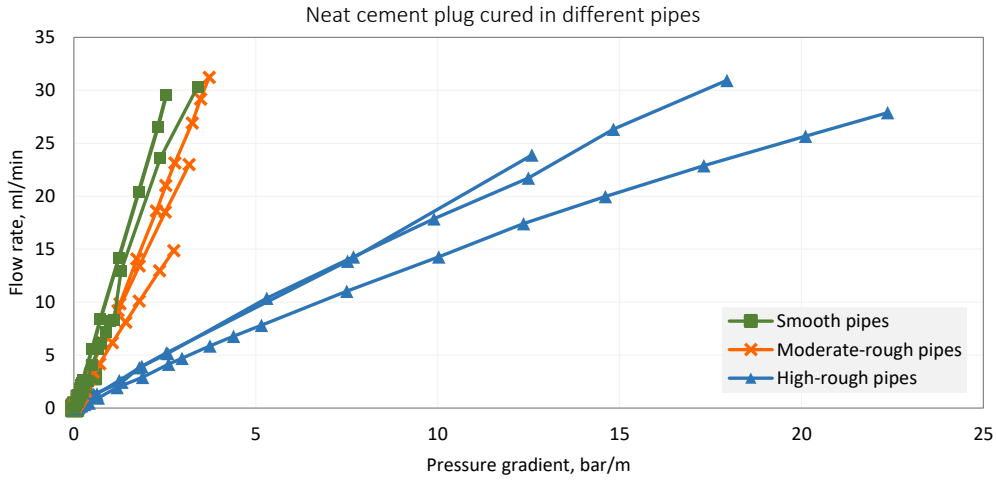

Fig. 4-6. Results of neat cement plug cured in different pipe roughness at T=66° C

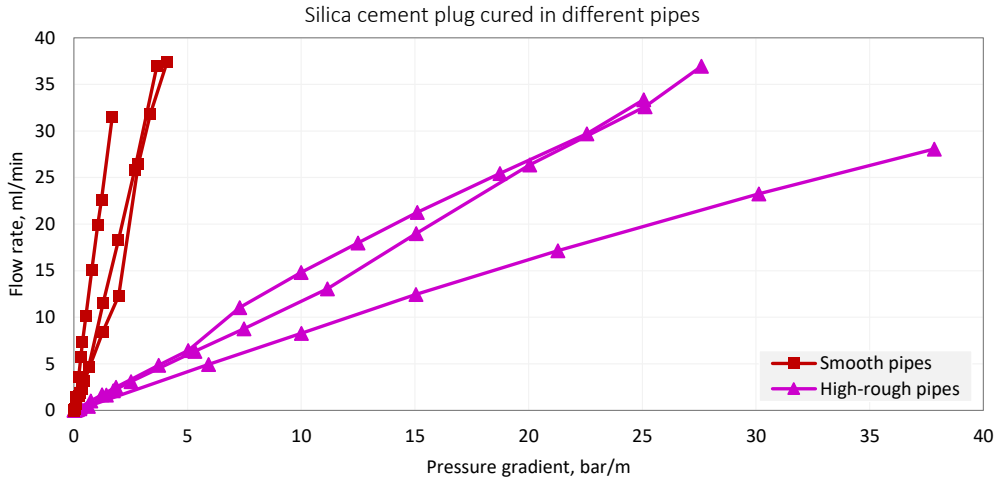

Fig. 4-7. Results of silica cement plug cured in different pipe roughness at T=120° C

Results from neat- and silica cement systems showed that samples cured in both rough pipes produced lower leak rates compared to those cured the smooth pipe. For the neat cement plug, the averaged leak rates of samples in the moderate- and high-rough pipe at ∇P = 2.5 bar/m were respectively 30% and 80% smaller than those cured in the smooth pipe. Whereas for the silica cement plug, the leak rate reduction of samples cured in the high-rough pipe was almost 90%. There was no apparent breakthrough pressure (<0.01 bar) measured in all test cases.

After the test, it was visually observed from the top side of the specimen that the source of the gas leak was located at the interface between cement and pipe, and no visible indication of leak through cement bulk was found (see Paper III). Furthermore, the gas permeabilities measured from cement cores of tested samples were 0.07 and 0.08 mD for neat- and silica cement, respectively. The flow rate in the sealed cement bulk (L=40 cm) was then estimated from gas permeability values by using Eq. 3-2. At ∇P= 2.5 bar/m, the flow rate was ~0.1 ml/min for both cement types, and it was considerably smaller than the test leak rate observed in Fig. 4-6 and Fig. 4-7. This observation validated the results from visual inspection, verifying that the flow through the cement bulk was not dominant. Hence, it was likely that leakage pathways at the cement/steel interface, or microannulus, were formed in the test samples. Further analysis of the influence of the pipe roughness to the cement plug hydraulic sealing is provided in Section 5. 2, which contains the investigation of fluid flow dynamics in the microannulus with different wall roughness.

4. 3 Effect of curing temperature and expanding agent on silica cement systems (Paper II)

4.3.1 Materials

Test cell pipes

Pipes used for this experiment were smooth pipes without a surface coating. The roughness of Ra of the pipes was ranging from 2-5 μm.

Cement systems

The type of cement system used in this experiment was silica cement. Three cement mixtures were prepared with Portland cement Class-G (NORCEM AS), 35% BWOC silica flour, and 62% BWOC water. One of the mixtures was prepared with an additional 2% expanding agent, which contained magnesium oxide. The curing conditions for each mixture are summarized in Table 4-5, and three parallel samples of each mixture were tested.

Table 4-5. Composition and curing properties of silica cement mixtures

Cement system	Cement composition			Curing condition		
	Water (% BWOC)	Silica flour (% BWOC)	Expanding agent (% BWOC)	Pressure (bar)	Temperature (ºC)	Curing period (days)
SF-66†)	62	35	-	20	66	4
SF-120	62	35	-	20	120	4
SF -120 + EA	62	35	2	20	120	4

†) This test result was based on the test of the silica cement system in the smooth surface casing in Section 4. 2. (Paper III)

4.3.2 Results and discussion

Effect of temperature

The comparison of results from samples SF-66 and SF-120 is plotted in Fig. 4-8. A clear difference was observed between these two systems as samples SF-66 formed curves with gentle slopes, while SF-120 samples formed curves with steep slopes. At ∇P=2.5 bar/m, the averaged leak rate of SF-66 samples (2.12 ml/min) was approximately ten times lower than that of SF-120 samples (22.5 ml/min). Furthermore, no clear breakthrough pressure (ΔP<0.01 bar) was observed in all samples, as also indicated in the previous comparative experiment.

Existing studies suggested that elevated curing temperature increases the reaction rate of (i) cement hydration and (ii) pozzolan reaction from silica flour (Jensen and Hansen 1999, Zhang et al. 2012), which could intensify autogenous shrinkage. Therefore, the increased leak rate of samples SF-120 might occur due to the escalated shrinkage.

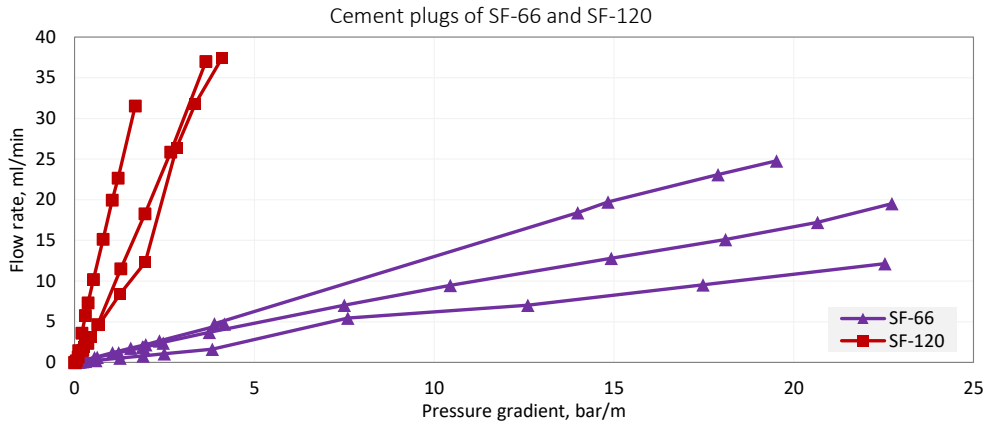

Fig. 4-8. Results of samples SF-66 and SF-120 plotted together

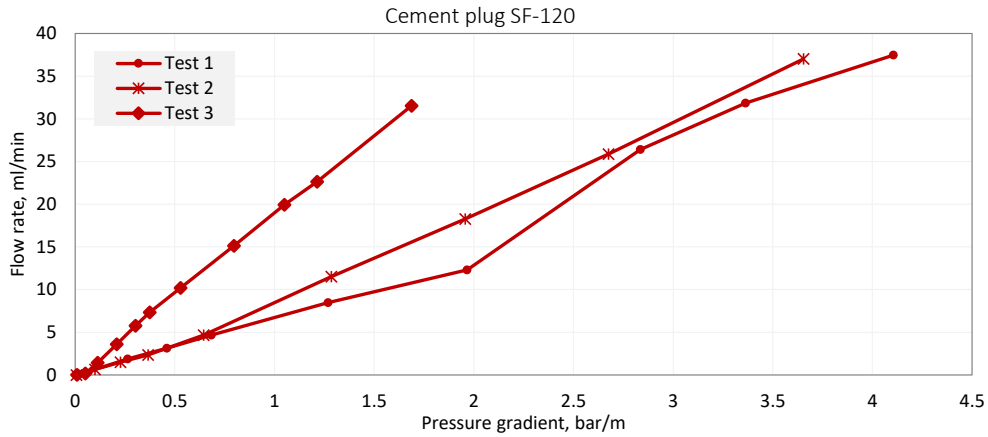

Fig. 4-9. Results of samples SF-120

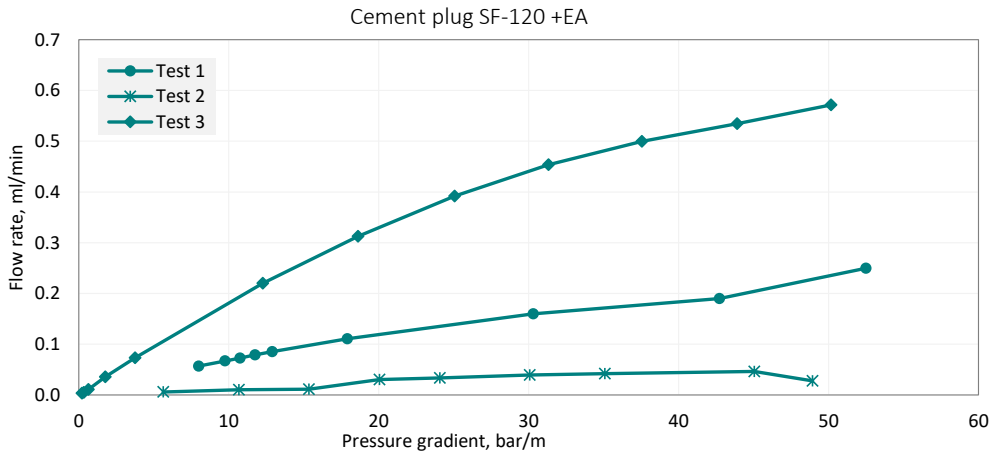

Fig. 4-10. Results of samples SF-120+EA. The first data point of ΔP from the samples SF-120 + EA were in the range of 0.03-3 bar

Effect of expanding agent

Results from samples SF-120 and SF-120+EA are shown in Fig. 4-9 and Fig. 4-10, respectively. It was observed that samples SF-120+EA had low leak rates, and the averaged leak rate at ∇P=10 bar/m was 0.12 ml/min. This value was considerably smaller than the averaged leak rate from samples SF-120, which was 127.3 ml/min (from linear extrapolation).

The breakthrough pressure of samples SF-120+EA could not be defined because the differential pressure at the beginning of the test could not be maintained constant, and consequently, the first data points of ΔP shown in Fig. 4-10 were slightly elevated. Furthermore, the visual inspection conducted on SF-120+EA samples after the test showed no signs of leaks.

The improved hydraulic sealing of samples with the expanding agent could be explained by the magnesium oxide contained in the expanding agent, which potentially contributed to counteract cement shrinkage. It was also presumed that the absence of a stabilizer in the SF-120+EA system might cause the free water and the expanding agent to segregate to the top of the cement slurry due to their low densities. Supposing that the segregation occurred, then the free water could increase the effectiveness of hydration of the expanding agent and improve the expansion, locally at the top of the cement plug.

Chapter 5
Fluid dynamics in microannuli

This chapter presents the study of the fluid flow dynamics in microannuli, simulated by using StarCCM+ (Siemens PLM Software 2017). The study was divided into two parts and presented separately in this chapter.

The first part of the study presents the fluid flow simulation of three fluid types flowing in two real microannuli, which was extracted from actual cement sheath samples, as presented in the examples by Vrålstad et al. (2019). Moreover, theoretical-based models of uniform microannuli were prepared for comparison.

The second part of the study focused on the investigation of fluid flow through uniform microannuli with three different wall roughness. This investigation was a continuation of the experimental study investigating the effect of the casing surface roughness on the cement plug hydraulic sealing (see Section 4. 2). It analyzes the mechanism behind the leak rate reduction observed in the cement plug placed in rough pipes. Furthermore, by using the key findings from the first part of the simulation work, the leak path characteristic of the test samples could be better described.

5. 1 Effect of microannuli geometries and fluid types on the fluid dynamics (Paper IV)

Microannulus is one of the typical leakage pathways that may present in the set cement. Several existing studies suggested that an actual microannuli have the characteristic of fracture-like nature in a brittle material, with a high variability of aperture sizes (De Andrade et al. 2014, De Andrade et al. 2016, Stormont et al. 2018, Garcia Fernandez et al. 2019, Vrålstad et al. 2019). This section presents the analysis of fluid dynamics of three different fluids – methane gas, water, and oil – flowing in two real microannuli. The 3D structures of the real microannuli were based on defects in two cement sheath samples – prepared from a separate experimental setup – and obtained by using X-Ray Computed Tomography (CT). As a comparison, theoretical uniform microannuli with three different apertures were also prepared. The investigated fluid dynamics were fluid flow streamlines, mass flow rate, and flow linearity.

5.1.1 Sample preparation and defects visualization of real microannuli

The investigated real microannuli were based on cement sheath samples that were molded in a space between a casing and a rock, as shown in Fig. 5-1. Without removing the cement sheath, the specimens were scanned by using an X-Ray CT. The 2D images from the scanning process were then processed and stacked to produce the final 3D volume of cement defects (Fig. 5-2). The defects found in the two cement sheath samples were mostly microannulus located at the interface between cement and casing.

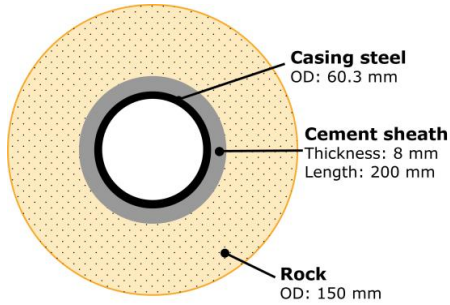

Fig. 5-1. The cross-section of the configuration for preparing the cement sheath samples

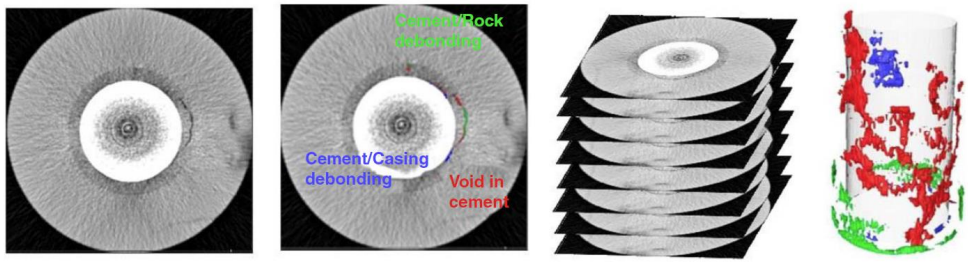

(a) (b) (c) (d)

Fig. 5-2. The process of extracting defects in the cement sheath by using an X-ray CT scan. (a) A 2D image, showing defects in the cement sheath. (b) Identification of defects in the cement sheath based on their location. (c) The stack of 2D CT scan images assembled into a 3D volume. (d) The final 3D volume of cement defects (Skorpa and Vrålstad 2018)

5.1.2 Microannuli geometries characterization

This section describes the morphology of (a) two real microannuli from the experimental samples and (b) uniform microannuli from the theoretical model, in sequence.

The microannulus of the first specimen (Fig. 5-3) was dominated by partial microannulus. At the front face, the microannulus was only located at the upper half (partial), whereas at the back face, the microannulus was vertically connected from the bottom to the top of the specimen with few casing/cement contacts present at the lower section. The aperture of the microannulus at the lower section was typically small (~1 mm), and it increased toward the upper section, with the largest aperture was located at the topmost of the back face (~6 mm).

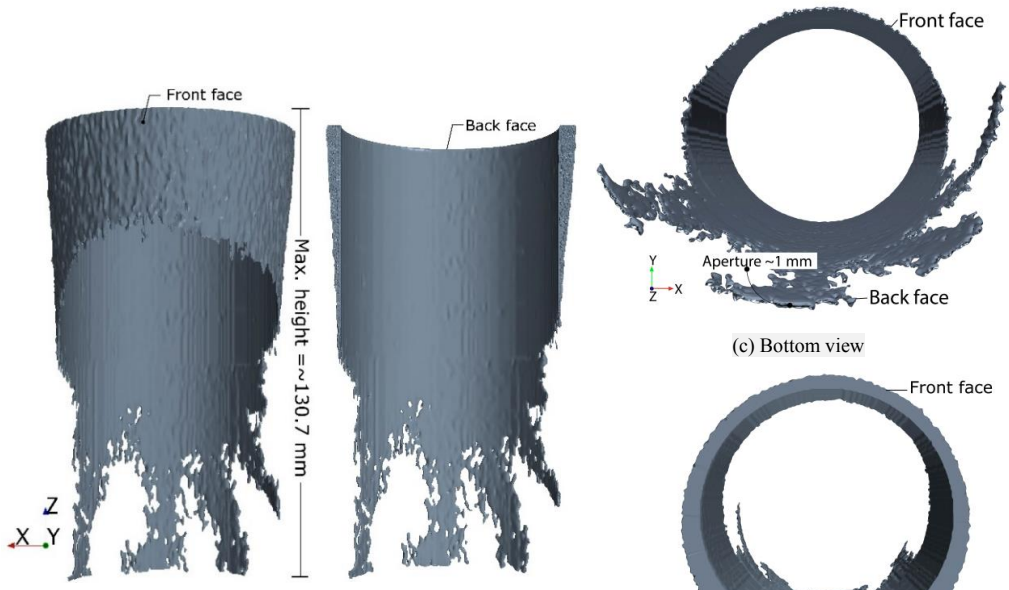

(a) Full geometry (b) With front-face culling (c) Bottom view (d) Top view

Fig. 5-3. The geometry of partial microannulus from the first specimen, viewed from the front (a and b), the bottom (c), and the top (d)

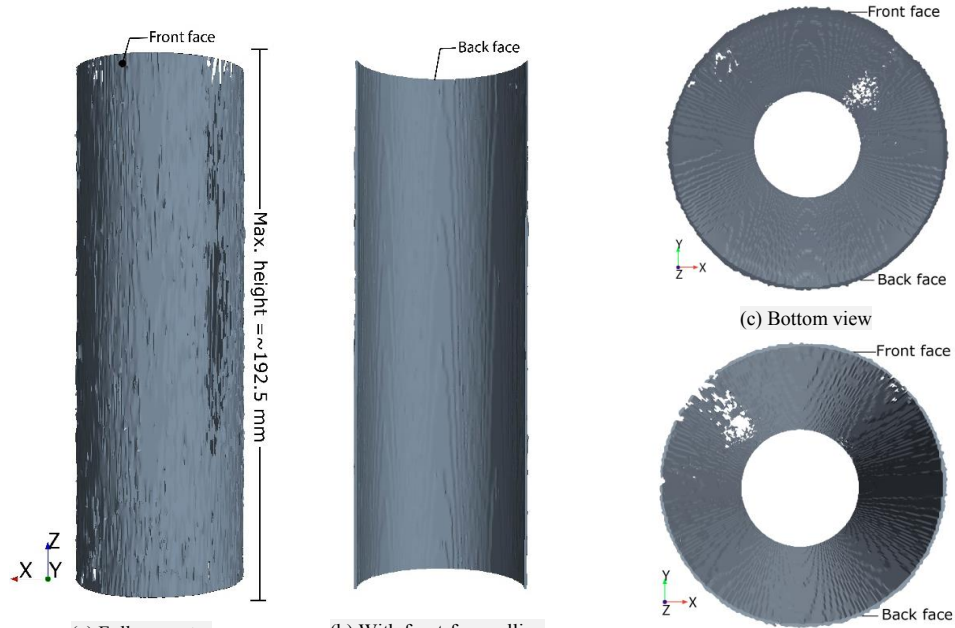

(a) Full geometry (b) With front-face culling (c) Bottom view (d) Top view

Fig. 5-4. The geometry of nearly complete microannulus from the second specimen, viewed from the front (a and b), the bottom (c), and the top (d)

The microannulus from the second specimen (Fig. 5-4) had the shape of a nearly-complete microannulus. It dominated the entire interface circumference and vertically connected from the bottom to the top side. At the front face, there were few casing/cement contacts present. The aperture of the microannulus was generally uniform at ~0.8 mm.

Three uniform microannuli were prepared, and they were modeled assuming complete microannulus shape, uniform aperture size, and smooth wall roughness. The aperture sizes of these microannuli were of 50 µm (Fig. 5-5), 350 µm, and 750 µm. The summary of all geometry cases from both experimental and theoretical microannuli is shown in Table 5-1.

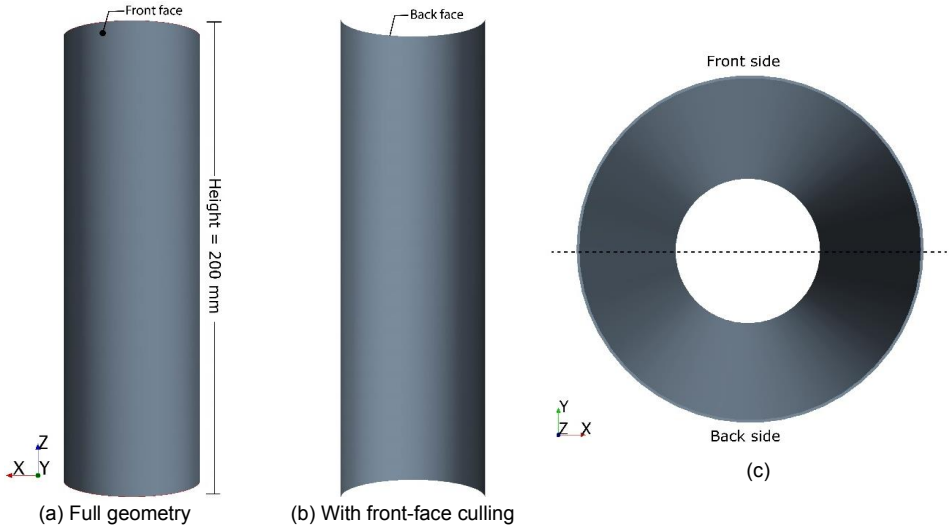

Fig. 5-5. The geometry of the uniform microannulus of 50 µm, viewed from the front (a and b) and the top (c)

Table 5-1.Summary of the simulation cases

Geometry case	Model	General descriptions
Case 1	Experimental (first specimen)	Partial microannulus
Case 2	Experimental (second specimen)	Nearly complete microannulus
Case 3	Theoretical	Uniform thickness of 50 µm
Case 4	Theoretical	Uniform thickness of 350 µm
Case 5	Theoretical	Uniform thickness of 750 µm

5.1.3 Simulation preparation

After the microannulus geometries were imported to the CFD software, the inlet and outlet areas were respectively defined at the bottom and the top side of the geometry and set as pressure-constant boundaries. The remaining regions of the geometry were set as a no-flow boundary. Afterward, the geometry was meshed with a trimmer mesher, polyhedral mesher, and prism layer mesher (five layers).

The fluid was assumed to have a constant density and flow in a laminar and steady-state condition. Furthermore, a segregated fluid flow solver was selected. In each geometry case,

three fluids of methane gas, water, and oil were simulated to flow, and the fluid properties of density and the kinematic viscosity (Table 5-2) were set based on the temperature of 120° C and pressure of 1 atm. In this study, the cement was assumed to be impermeable, so the fluid only flowed through the microannulus.

The simulation was run at multiple differential pressures, ranging from 20-500 Pa. Accordingly, the inlet pressure was changed repeatedly, while the outlet pressure was kept constant at atmospheric conditions. The simulation was run until the solution converged.

Table 5-2.Summary of the density and kinematic viscosity of the simulated fluids at T=120° C and P=1 atm

Fluid type	Density (kg/m^3)	Kinematic viscosity (Pa-s)
Methane gas	0.4911	14.09 x 10^{-6}
Water	940.7	2.25 x 10^{-4}
Oil	710	3.5 x 10^{-3}

5.1.4 Results

Real microannuli: Case 1 and Case 2

The results of fluid flow streamlines and velocity of methane gas at ∇P=2.5 kPa/m are shown in Fig. 5-6 and Fig. 5-7, respectively, for Case 1 and 2. The results from partial microannulus of Case 1 showed that channeling streamlines were mainly presented at the lower part of the back face, giving the indication of tortuous fluid flow (Fig. 5-6b). This tortuous flow also has a significant variation in velocity, presumed due to non-uniform microannulus apertures. At the upper part of the back face, parallel and straight streamlines with high fluid velocity were

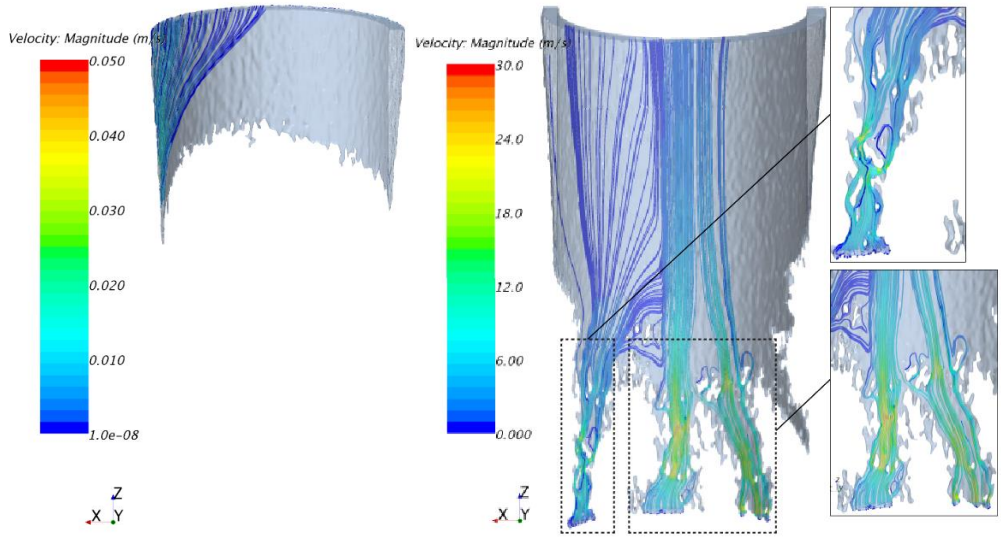

(a) (b)

Fig. 5-6. The flow streamlines of methane gas at ∇P=2.5 kPa/m through the microannulus of Case 1 at (a) the front face and (b) the back face. Note that each microannulus face has a different range of fluid velocity.

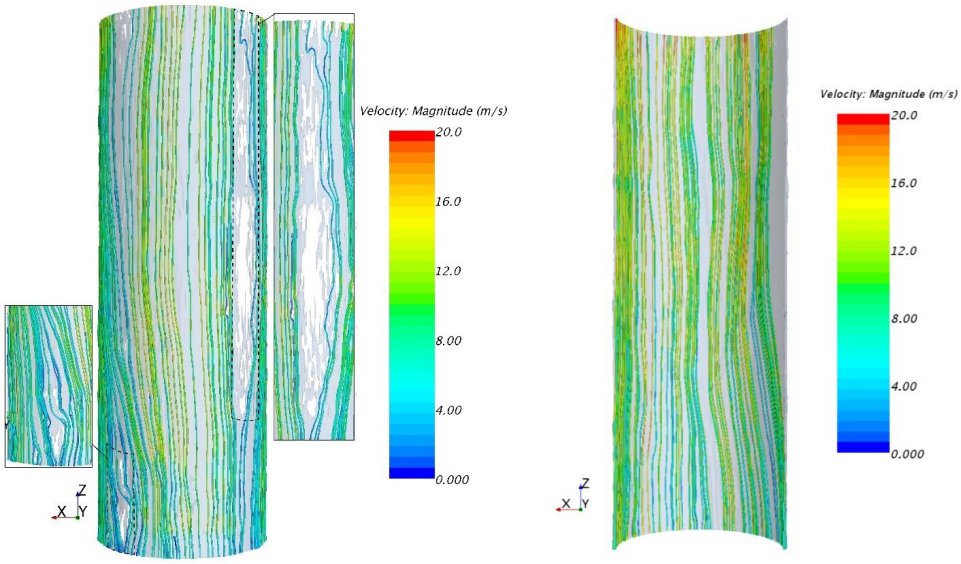

Fig. 5-7. The flow streamlines of methane gas at ∇P=2.5 kPa/m through the microannulus of Case 2 at (a) the front face and (b) the back face

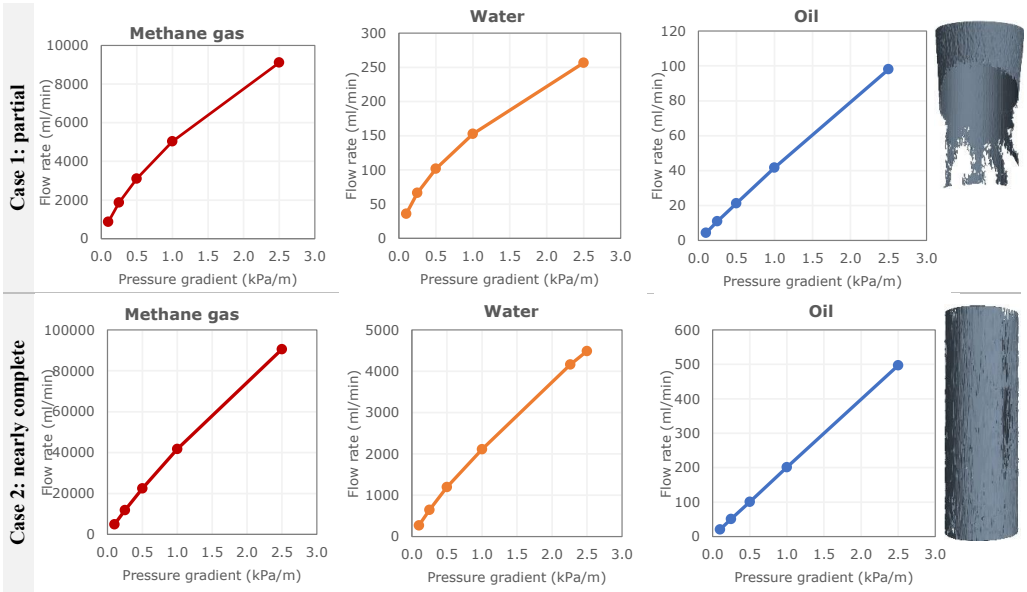

Fig. 5-8. Plots of ∇P vs. Q flowrate for all types of fluids from geometry cases of real microannuli

concentrated in the middle area (or highway area), and transverse streamlines were indicated on the sides. The highly-connected microannulus and relatively large aperture in the highway area were likely to cause fluid to flow rapidly.

Fluid flow streamlines in the nearly-complete microannulus of Case 2 were mostly parallel along the flow direction with wavy features at both faces. A hint of channeling flow was observed at the area on the front face, where contacts between casing/cement were present (Fig.

5-7a). Variation in velocity was observed at both faces, although it was less significant in value than that of the partial microannulus of Case 1.

The plots of ∇P vs. Q from the simulation results of each fluid type are shown in Fig. 5-8, for both Case 1 and Case 2. According to the plots, methane gas and water flowing through both real microannuli produced non-linear curves, while only oil fluid produced a linear relationship.

Theoretical microannuli: Case 3-5

The results of fluid flow streamlines and fluid velocity of water at ∇P=2.5 kPa/m for theoretical microannulus Case 3-5 are shown in Fig. 5-9. The flow streamlines in all these three cases were identical, with perfectly straight and parallel streamlines along the flow direction. There was no significant variation of velocity observed in these three cases, which was expected due to the uniform microannulus aperture and the smooth surface.

The plots of ∇P vs. Q from the simulation results of each fluid type are shown in Fig. 5-10, for all cases. It was observed that all fluids flowing through these three uniform microannuli produced linear curves, with the only exception from water flow in the microannulus with an aperture of 750 µm (Case 5).

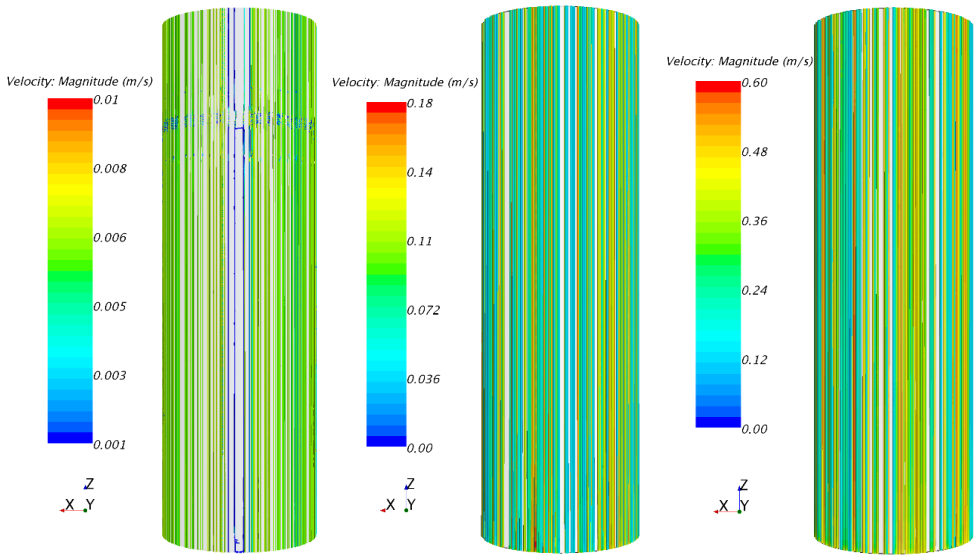

(a) (b) (c)

Fig. 5-9. The flow streamlines of water at ∇P=2.5 kPa/m through the microannulus of (a) Case 3, (b) Case 4, and (c) Case 5 at the front face. Note that each case has a different range of fluid velocity.

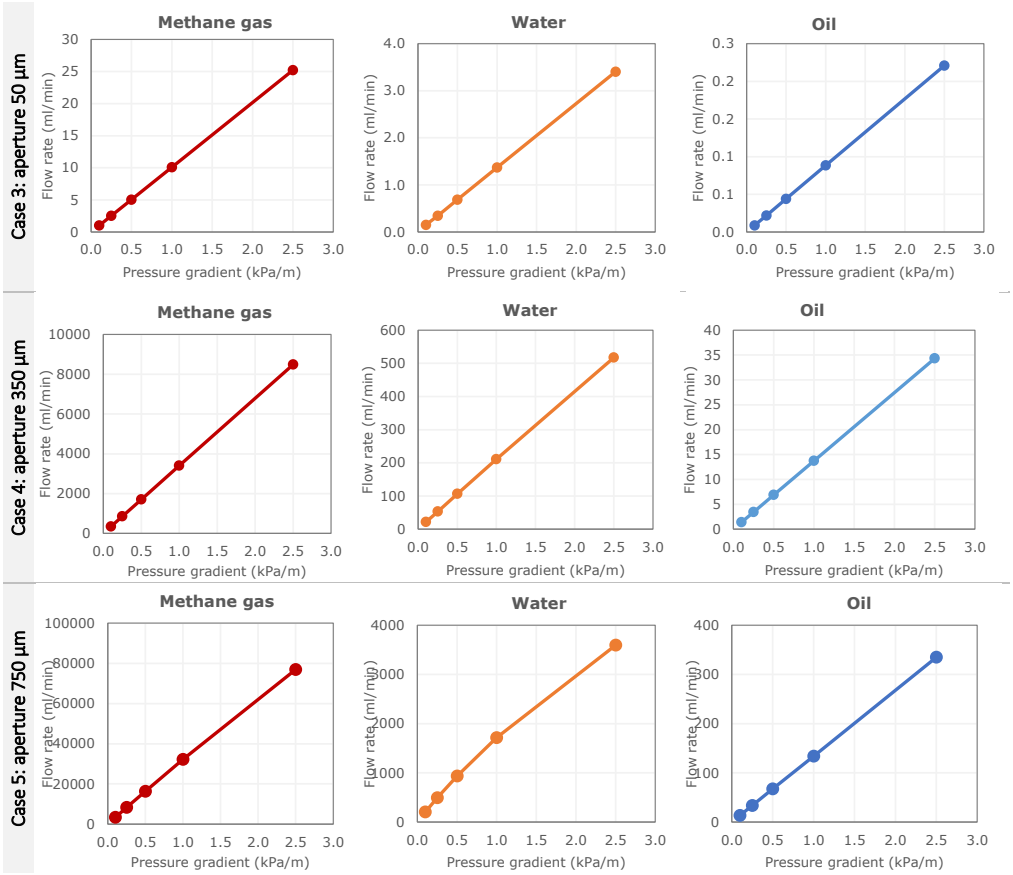

Fig. 5-10. Plots of ∇P vs. Q for all type of fluids from geometry cases of theoretical microannuli

5.1.5 Discussions

Forchheimer number criterion

In the linear Darcy flow, the flow rate is linearly correlated with the pressure gradient (see Eq. 3-2). However, the linear Darcy flow could be terminated if the fluid flow rate was large or significant inertial effect emerged. To account for these effects, Forchheimer (1901) added a second-order term explaining this non-linear behavior, expressed as:

$$-\nabla P = AQ + BQ^2 \qquad \text{(Eq. 5-1)}$$

$$-\nabla P = \frac{\mu}{kA_h}Q + \frac{\beta\rho}{A_h^2}Q^2 \qquad \text{(Eq. 5-2)}$$

where A and B are respectively the coefficients describing energy losses due to the viscous and inertial dissipation mechanisms, ρ is the fluid density (kg/m^3), and β is called the non-Darcy coefficient. The coefficient A represents the intrinsic permeability of the crack, and the coefficient B is dependent on the geometrical properties of the media.

Following the Forchheimer equation, the criteria of termination of linear Darcy flow can be established by calculating the Forchheimer number, F_o (Zeng and Grigg 2006, Chen et al. 2015):

$$Fo = \frac{BQ^2}{AQ} = \frac{BQ}{A} \quad \text{(Eq. 5-3)}$$

In this analysis, F_o> 0.11 was defined as the criteria for the flow to enter the non-Darcy flow zone (Zeng and Grigg 2006). The summary of the averaged F_o for each case and fluid types is shown in Table 5-3.

Table 5-3.Summary of Forchheimer number for all simulated cases and fluid types

Model	Cases	Averaged Forchheimer number		
		Methane gas	Water	Oil
Experimental	Case 1	0.74 †)	2.17 †)	0.04
	Case 2	0.13 †)	0.17 †)	0.01
Theoretical	Case 3	1 x 10^{-6}	3.7 x 10^{-3}	-1.5 x 10^{-4} ‡)
	Case 4	1.5 x 10^{-3}	0.01	3.3 x 10^{-5}
	Case 5	0.03	0.17 †)	7 x 10^{-4}

†) Forchheimer number exceeds the critical value of 0.11
‡) Negative sign indicates the linear-Darcy flow is dominant

Methane gas and water flowing in both real microannuli Case 1 and Case 2 returned F_o > 0.11, indicating non-linear Darcy flow applied. Meanwhile, oil in both real microannuli was found to flow in linear Darcy because of fairly low F_o values: 0.04 and 0.01, respectively, for Case 1 and Case 2. These observations implied that the inertial effect was more dominant in low-viscous fluid flow, while it became less dominant in high-viscous fluid flow due to the increased viscous effect. The analysis based on F_o criterion matched with the observation of curve linearity in plot of ∇P vs. Q (Fig. 5-8).

The averaged F_o of each fluid from the partial microannulus geometry of Case 1 was larger than that from the nearly-complete microannulus geometry of Case 2. Increased F_o value could be attributed to (i) frequent flow acceleration and deceleration, which could be indicated from variation in velocity, and (ii) tortuous fluid flow (Chen et al. 2015, Zou et al. 2017). As observed in the fluid flow streamline results in Fig. 5-6 (Case 1) and Fig. 5-7 (Case 2), these attributes were more significant in fluid flow in Case 1 than in Case 2.

All fluids flowing through all theoretical microannuli cases returned low values of F_o<0.11, except for water in Case 5 with F_o of 0.17. The low F_o values signified that the inertial effect of fluid flow in the uniform microannulus was insignificant, as confirmed by the observation of fluid streamlines results (Fig. 5-9). Furthermore, the large F_o value of water flow in Case 5 was likely intensified by the high fluid flow rates and water density.

Comparison of fluid dynamics of real and uniform microannuli

Based on plots of ∇P vs. Q, most fluids in the theoretical microannuli had linear flow (Fig. 5-10), and this was similar to the oil flow in the real microannuli (Fig. 5-8). Nevertheless, this observation not necessarily implied that theoretical microannuli was accurate to simulate the overall fluid flow phenomena of the real microannuli. For example, the flow streamlines in the real microannuli were likely to be tortuous with velocity variation, particularly if frequent contacts of cement/casing present in the microannulus.

In addition to that, the assumption of homogenous aperture and complete-microannulus shape of the theoretical models might oversimplify the morphology of real microannuli. For example, the partial microannulus from the experimental model Case 1 was nowhere similar to the shape of a complete microannulus. It also had a wide-ranged aperture, which might not be accurate to be defined by a single-valued hydraulic aperture.

5. 2 Effect of wall roughness of uniform microannuli on the fluid dynamics (Paper III)

The microannuli used in this simulation was only an approximation of the shape of microannuli indicated in the experimental tests because the actual microannulus could not be obtained from the cement plug samples. The simulation was performed replicating the operating condition of the experiment in Section 4. 2 to obtain these results: (a) the equivalent microannuli width estimated from the leak rate measured in the experimental tests and (b) fluid flow visualization.

5.2.1 Microannuli models characterization

The leak path models were created as a shape of complete-microannuli with uniform-gap width, encircling the interface between cement and steel. The microannuli wall roughness was assumed identical to the surface roughness of the test pipes (Table 4-2), and hence theoretical models with three levels of wall roughness, (a) smooth, (b) moderate-rough, and (c) high-rough, were prepared (Fig. 5-11). Additional information about sensitivity analysis for choosing the models could be found in Appendix A.1.

5.2.2 Simulation preparation

The models were then imported into the CFD software. The bottom- and top regions of the geometry were assigned as the fluid inlet and outlet, respectively. They were set as a constant pressure boundary, and the remaining regions were set as a no-flow boundary. A trimmed mesher with six layers of prism layers close to the wall was selected as the volume mesher.

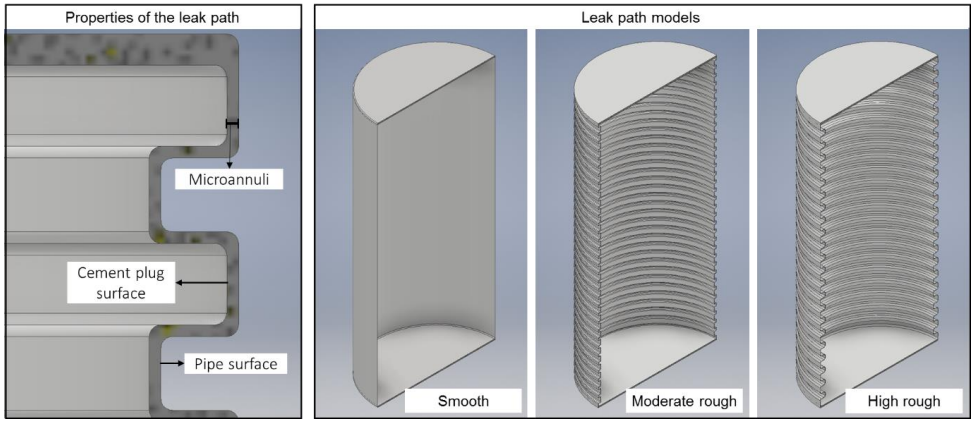

Fig. 5-11. (Left) Description of the microannuli model and (right) the cross-section of microannuli models with three different wall roughness

The fluid was assumed nitrogen gas (relevant to the experiment) with the constant density. The fluid flow was assumed laminar and steady-state, and the flow solver was segregated flow model. Simulations were run until the residual values reached convergence.

At first, the simulation was run to estimate the aperture of uniform microannuli, which flow rates equivalent to the test leak rates in all test cases (Table 4-4). The wall roughness of the microannuli in each simulated case was set accordingly based on the surface roughness of the test pipe. Then, the mass flow was calculated at five values of differential pressures, achieved by setting a constant inlet pressure at 20 bar and by changing the outlet pressure repeatedly. The equivalent microannulus aperture was estimated until the mass flow output matched the averaged experimental leak rates with less than 1% deviation.

Afterward, another simulation was run on three microannulus models – one model for each level of wall roughness – with the same aperture of 0.1 mm. The simulation was run to obtain mass flow and fluid flow visualization at a differential pressure of 1 bar – i.e. the inlet- and outlet pressure was set at 20 and 19 bar, respectively.

In all simulations, the density (ρ) and dynamic viscosity (μ) of the nitrogen were assumed to be constant at a pressure of 20 bar, and depending on the test temperature they were set as follow:

- At T=66^o C, ρ=19.85 kg/m^3 and μ= 19.89 x 10^{-4} Pa-s, and
- At T=120^o C, ρ=17.06 kg/m^3 and μ=22.1 x 10^{-6} Pa-s.

5.2.3 Results and discussion

Results presented and discussed in this section used the example of simulation results run at T=66^o C (relevant for the experiment of neat cement system), and the remaining results are

provided in Appendix A.2. This was to avoid confusion because the overall results shared similar characteristics. The equivalent microannuli estimated from the leak rate of the experimental test are summarized in Table 5-4, and the ∇P vs. Q curves from the simulation and the experimental results were plotted together, shown in Fig. 5-12.

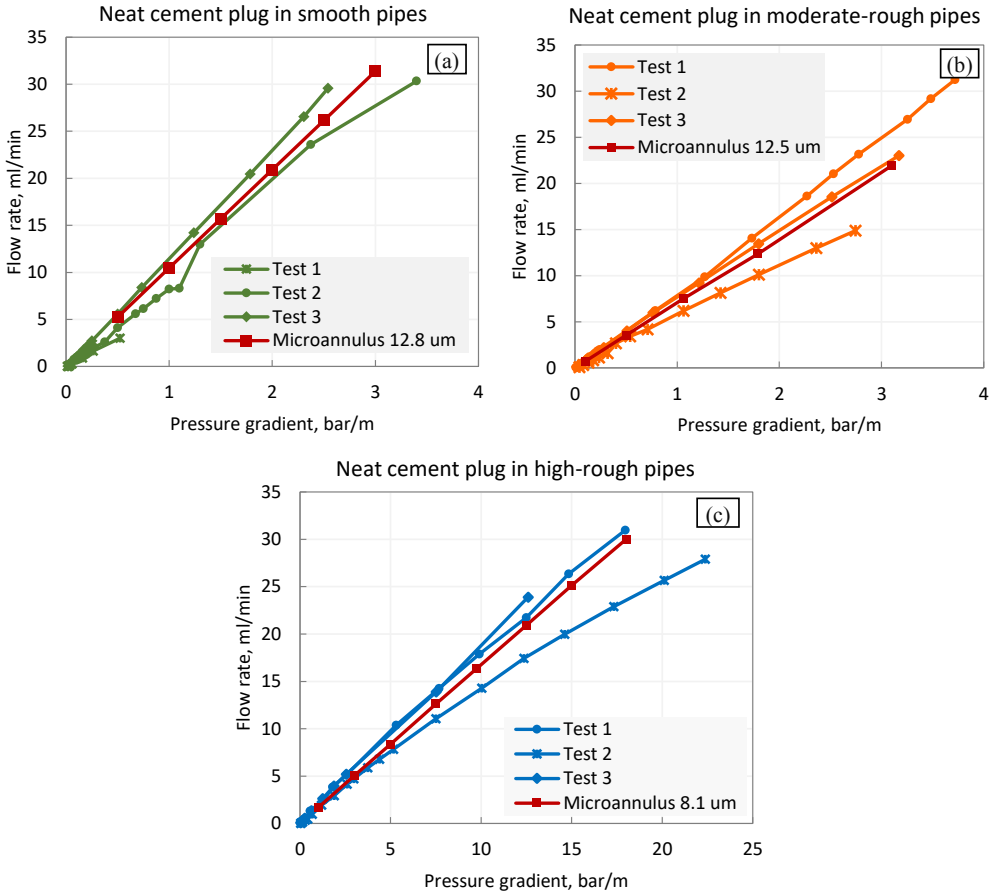

Fig. 5-12. Plots of ∇P vs. Q from the experimental test of neat cement systems (T=66° C), plotted together with uniform microannulus results from the fluid dynamics simulation

Table 5-4. Summary of the equivalent microannulus aperture based on experimental results of neat cement

Test pipes	Equivalent microannuli width*)
Smooth	12.8 μm
Moderate rough	12.5 μm
High rough	8.1 μm

*) The presented value has a 1-digit of decimal precision to produce a mass flow rate with <1% deviation

The mass flow rates from the microannulus models with an aperture of 0.1 mm are summarized in Table 5-5. It was observed that the fluid flow rate in the smooth microannulus was the highest. On the other hand, the mass flow rate in both of the rough-surface microannuli

was reduced by ~70 %. This reduction was presumably caused by the tortuous fluid streamlines indicated only in the rough-surface microannuli (Fig. 5-13).

Table 5-5. Summary of mass flow through microannuli (width=0.1 mm) with different roughness computed from the fluid simulation at a differential pressure of 1 bar and temperature 66° C

Leak path models	Mass flow rate (kg/s)
Smooth	11.01 x 10^{-3}
Moderate rough	3.01 x 10^{-3}
High rough	3.50 x 10^{-3}

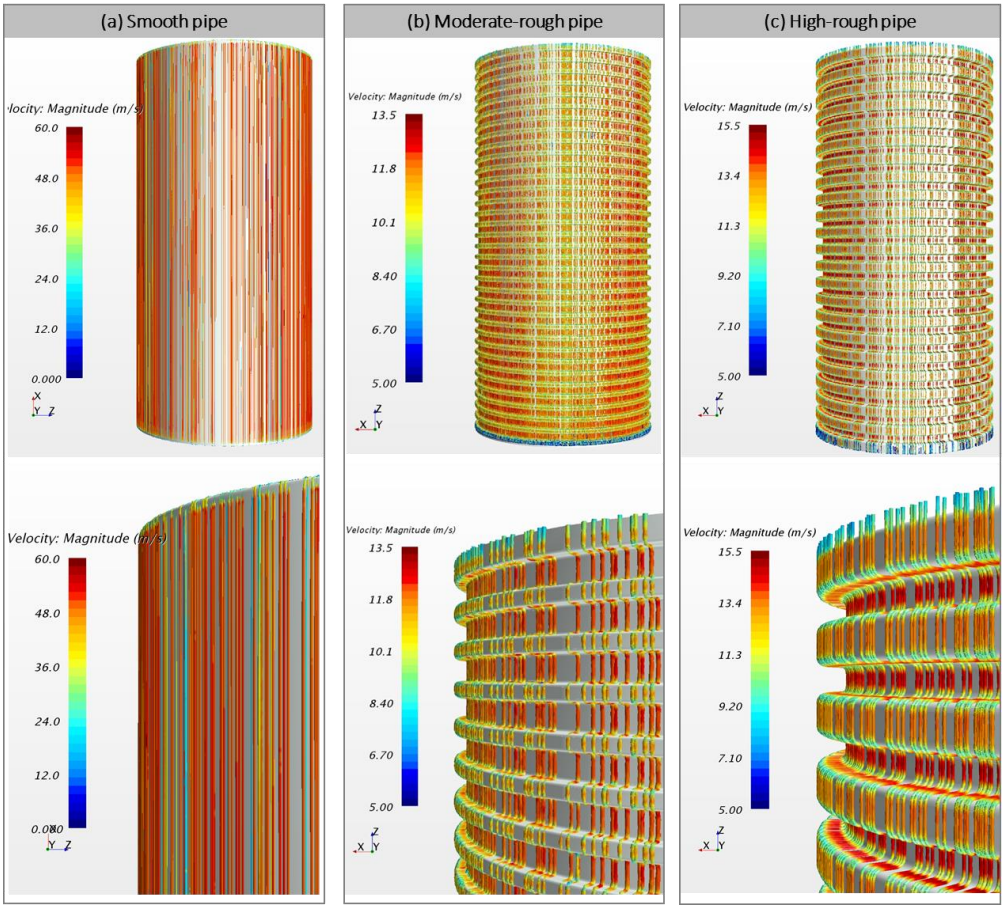

Fig. 5-13. Scalar plot of gas velocity through leak path models of (a) smooth, (b) moderate-rough, and (c) high-rough. The grey area represents the surface of the cement plug periphery, and the pipe is transparent.

Although the simulated microannuli model was only theoretical, the observation from the simulation results could give an indication that there might be an increased tortuosity of the actual microannuli in the test samples placed in the rough pipes that added resistance fluid to flow. Refer to the results in Chapter 5. 1, the actual microannuli morphology formed in the cement plug samples might be predicted based on the flow behavior from plots of ∇P vs. Q (Fig. 5-12). It was observed that samples placed in the smooth and moderate-rough pipes

generated linear relationship, indicating that the actual microannuli could be highly connected, with a tendency to shape a complete microannuli. On the other hand, samples placed in the high-rough pipes generate non-linear curves, indicating that the tortuous flow through the actual microannuli could be significant due to irregular and complex leak path shapes, such as partial microannuli or connected cracks.

Chapter 6
Conclusions and recommendations

6. 1 Conclusions

This thesis reports an investigation of the hydraulic integrity of the cement plug by using a test setup for assessing the sealing performance of cement to pipe and linking it with several influencing parameters. In addition, it includes the analysis of the fluid flow dynamics in microannuli. The conclusions from this research work are as follows:

- The small-scale apparatus for the hydraulic sealing test is found to be functional in testing a cement plug. The baseline result is established based on the test of Portland cement Class-G with no additives, prepared with the dry-cured method.
- The cement curing condition influences the cement sealing results. Samples prepared with the dry-cured method have low breakthrough pressure (<0.01 bar). Results from the comparative tests, which also run with the dry-cured method, show similar observation of low breakthrough pressure. On the contrary, samples prepared with the wet-cured method are observed with high breakthrough pressure (~10 bar).
- The first comparative experiment shows that placing the cement plug next to the rough-surface casing reduces the gas leak rate, and this applies for both neat- and silica cement. The analysis of fluid flow simulation in uniform microannuli with different wall roughness, which is based on this first comparative experiment, suggests that the leak rate reduction found from samples cured in rough-surface casings is due to the increased microannuli tortuosity. Furthermore, non-linear curves of ∇P vs. Q of test samples cured in high-rough casing give an indication of low-connectivity microannuli.
- The second comparative experiment shows that silica cement plug cured at elevated temperature (120^{o} C) experienced more leakage than that cured at low temperature (66^{o} C). Adding an expanding agent is found to significantly reduce the high leak rates of silica cement plug at elevated temperature. Post-examinations show that adding an expanding agent can contribute to preventing the formation of microannuli from shrinkage.
- The fluid flow in the investigated real microannuli is likely complex because of the inhomogeneous features of microannuli morphology (e.g. non-uniform aperture and irregular roughness). The observed increase in the inertial effect of non-linear flow could be attributed to (i) the low viscosity of flowing fluid and (ii) increased in the

complexity of microannulus geometry. This observation is validated by the Forchheimer number criterion.

- The theoretical-based model of a uniform microannulus may give limitations in representing the fluid flow phenomena in the real microannuli because the assumptions of homogenous aperture and smooth surface are too simplistic and may oversimplify the non-homogenous morphology of the real microannuli.

6. 2 Recommendations

The following are several aspects of the current topic that can be addressed in future works:

- The leak observation in the cement plug samples suggested that the possible failure mechanism is due to cement shrinkage. Numerical simulation of stress calculation in cement plug can be a supplementary analysis to validate the results and study the crack propagation in cement plug, e.g., radial or axial cracking. Models that consider the coupling between the hydraulics (fluid pressure) and mechanics (mechanical properties of solid materials), such as in Bois et al. (2019), might be relevant to the loading mechanism in the cement plug hydraulic sealing test.
- Further experimental tests shall investigate other improved cement systems, or other types of plugging material, for addressing the cement shrinkage issue.
- The current experiment of cement plug hydraulic integrity test was conducted on a small-scale testing apparatus. Therefore, verifying the validity of the results for the field performance means the need to conduct the experiments at an in-situ scale. This approach may also be beneficial to establish correlations between results from downscaled and in-site scaled, which was still limited to be found in the existing research.
- Observation of defects in the cement plug in this research work can be improved to get more details on the microannuli morphology, for example, by replacing the steel casing with titanium casing so X-ray CT scans can be performed on the cement plug samples.
- The model for fluid flow dynamic simulation can be improved with a model that consists of both cement and microannuli (or other types of defects), and hence fluid can be simulated to also flow in cement pores (see Paper IV). Moreover, multiple fluid phases may be included in the simulation to analyze capillary pressure.

References

Aas, Bjarne, Sørbø, Jostein, Stokka, Sigmund et al. 2016. Cement Placement with Tubing Left in Hole during Plug and Abandonment Operations. Presented at the IADC/SPE Drilling Conference and Exhibition, Fort Worth, Texas, USA. 2016/3/1/. https://doi.org/10.2118/178840-MS.

Abshire, Lucas W, Desai, Praful, Mueller, Dan et al. 2012. Offshore permanent well abandonment. *Oilfield Review* **24** (1): 42-50.

Akgün, Haluk and Daemen, Jaak JK. 1999. Design implications of analytical and laboratory studies of permanent abandonment plugs. *Canadian Geotechnical Journal* **36** (1): 21-38.

Barclay, Ian, Pellenbarg, Jan, Tettero, Frans et al. 2001. The beginning of the end: a review of abandonment and decommissioning practices. *Oilfield Review* **13** (4): 28-41.

Bois, Axel-Pierre, Garnier, Andre, Rodot, Francois et al. 2011. How To Prevent Loss of Zonal Isolation Through a Comprehensive Analysis of Microannulus Formation. *SPE Drilling & Completion* **26** (01): 13-31.

Bois, Axel-Pierre, Vu, Manh-Huyen, Noël, Kim et al. 2019. Evaluating Cement-Plug Mechanical and Hydraulic Integrity. *SPE Drilling & Completion* **34** (02): 92-102. https://doi.org/10.2118/191335-PA.

Boukhelifa, L., Moroni, N., James, S. G. et al. 2004. Evaluation of Cement Systems for Oil and Gas Well Zonal Isolation in a Full-Scale Annular Geometry. Presented at the IADC/SPE Drilling Conference, Dallas, Texas. 2004/1/1/. https://doi.org/10.2118/87195-MS.

Carter, L. G. and Evans, G. W. 1964. A Study of Cement-Pipe Bonding. *Journal of Petroleum Technology* **16** (02): 157-160.

Chen, Yi-Feng, Zhou, Jia-Qing, Hu, Shao-Hua et al. 2015. Evaluation of Forchheimer Equation Coefficients for Non-Darcy Flow in Deformable Rough-Walled Fractures. *Journal of Hydrology* **529**: 993-1006. http://www.sciencedirect.com/science/article/pii/S0022169415007040.

CSI Technologies. 2011. Cement Plug Testing: Weight vs. Pressure Testing to Assess Viability of a Wellbore Seal Between Zones. Report No. TAP-680, Bureau of Safety and Environmental Enforcement, Washington DC (2011).

Daccord, Gérard , Guillot, Dominique, and James, Simon 2006. Remedial Cementing. In *Well Cementing*, ed. E. B. Nelson and Dominique Guillot. Sugar Land, Texas: Schlumberger.

De Andrade, J., Torsaeter, M., Todorovic, J. et al. 2014. Influence of Casing Centralization on Cement Sheath Integrity During Thermal Cycling. Presented at the IADC/SPE Drilling Conference and Exhibition, Fort Worth, Texas, USA. 2014/3/4/. https://doi.org/10.2118/168012-MS.

De Andrade, Jesus, Sangesland, Sigbjorn, Skorpa, Ragnhild et al. 2016. Experimental Laboratory Setup for Visualization and Quantification of Cement-Sheath Integrity. *SPE Drilling & Completion* **31** (04): 317-326. https://doi.org/10.2118/173871-PA.

Duguid, Andrew, Butsch, Robert, Carey, J. William et al. 2013. Pre-injection Baseline Data

Collection to Establish Existing Wellbore Leakage Properties. *Energy Procedia* **37**: 5661-5672. http://www.sciencedirect.com/science/article/pii/S1876610213007315.

Eilers, L. H. and Root, R. L. 1976. Long-Term Effects of High Temperature on Strength Retrogression of Cements. Presented at the SPE California Regional Meeting, Long Beach, California. 1976/1/1/. https://doi.org/10.2118/5871-MS.

Evans, George W. and Carter, L. Gregory. 1962. Bounding Studies of Cementing Compositions to Pipe and Formations. January 1, 1962.

Forchheimer, P. 1901. Wasserbewegung durch Boden. *Zeitz ver Deutsch Ing* **45**: 1782-1788.

Garcia Fernandez, Serafin, Matteo, Edward N., Taha, Mahmoud Reda et al. 2019. Characterization of wellbore microannuli. *Journal of Natural Gas Science and Engineering* **62**: 13-25. http://www.sciencedirect.com/science/article/pii/S1875510018305316.

Gasda, Sarah E., Celia, Michael A., Wang, James Z. et al. 2013. Wellbore Permeability Estimates from Vertical Interference Testing of Existing Wells. *Energy Procedia* **37**: 5673-5680. http://www.sciencedirect.com/science/article/pii/S1876610213007327.

Gaurina-Međimurec, Nediljka, Sedić, Krunoslav, Čajić, Anel et al. 2017. Effect of Microblock on the Compressive Strength of Portland Cement at Elevated Temperatures. V008T11A041. https://doi.org/10.1115/OMAE2017-62455.

Ghofrani, Reza and Plack, Heiko. 1993. CaO- and/or MgO-Swelling Cements: A Key for Providing a Better Annular Sealing? Presented at the SPE/IADC Drilling Conference, Amsterdam, Netherlands. 1993/1/1/. https://doi.org/10.2118/25697-MS.

Goodwin, K. J. and Crook, R. J. 1992. Cement Sheath Stress Failure. *SPE Drilling Engineering* **7** (04): 291-296. https://doi.org/10.2118/20453-PA.

Grabowski, E. and Gillott, J. E. 1989. Effect of replacement of silica flour with silica fume on engineering properties of oilwell cements at normal and elevated temperatures and pressures. *Cement and Concrete Research* **19** (3): 333-344. http://www.sciencedirect.com/science/article/pii/0008884689900239.

Jackson, P. B. and Murphey, C. E. 1993. Effect of Casing Pressure on Gas Flow Through a Sheath of Set Cement. Presented at the SPE/IADC Drilling Conference, Amsterdam, Netherlands. 1993/1/1/. https://doi.org/10.2118/25698-MS.

Jensen, Ole Mejlhede and Hansen, Per Freiesleben. 1999. Influence of temperature on autogenous deformation and relative humidity change in hardening cement paste. *Cement and Concrete Research* **29** (4): 567-575. http://www.sciencedirect.com/science/article/pii/S0008884699000216.

Kaiser, Mark J. 2017. Rigless well abandonment remediation in the shallow water U.S. Gulf of Mexico. *Journal of Petroleum Science and Engineering* **151**: 94-115.

Khalifeh, Mahmoud, Akbari, Babak, Khan, Ahsan et al. 2019. A Critical Review of Rules and Regulations for Permanently Plugged and Abandoned Wells. *Proc.,* ASME 2019 38th International Conference on Ocean, Offshore, and Arctic Engineering, Glasgow, United Kingdom.

Khalifeh, Mahmoud, Hodne, Helge, Saasen, Arild et al. 2018. Bond Strength Between Different Casing Materials and Cement. Presented at the SPE Norway One Day Seminar, Bergen, Norway. 2018/4/18/. https://doi.org/10.2118/191322-MS.

Khalifeh, Mahmoud, Hodne, Helge, Saasen, Arild et al. 2013. Techniques and Materials for

North Sea Plug and Abandonment Operations. Presented at the Offshore Technology Conference, Houston, Texas, USA. 2013/5/6/. https://doi.org/10.4043/23915-MS.

King, George Everette and Valencia, Randy L. 2014. Environmental Risk and Well Integrity of Plugged and Abandoned Wells. Presented at the SPE Annual Technical Conference and Exhibition, Amsterdam, The Netherlands. 2014/10/27/. https://doi.org/10.2118/170949-MS.

Kiran, Raj, Teodoriu, Catalin, Dadmohammadi, Younas et al. 2017. Identification and evaluation of well integrity and causes of failure of well integrity barriers (A review). *Journal of Natural Gas Science and Engineering* **45**: 511-526. http://www.sciencedirect.com/science/article/pii/S1875510017302184.

Liversidge, D., Taoutaou, S., and Agarwal, S. 2006. Permanent Plug and Abandonment Solution for the North Sea. Presented at the SPE Asia Pacific Oil & Gas Conference and Exhibition, Adelaide, Australia. 2006/1/1/. https://doi.org/10.2118/100771-MS.

Mainguy, M., Longuemare, P., Audibert, A. et al. 2007. *10.2516/ogst:2007026*. Analyzing the Risk of Well Plug Failure after Abandonment. *Oil & Gas Science and Technology - Rev IFP* **62** (3): 311-324. https://doi.org/10.2516/ogst:2007026.

Nagelhout, Alexander, Bosma, Martin G. R., Mul, Paul et al. 2010. Laboratory and Field Validation of a Sealant System for Critical Plug-and-Abandon Applications. *SPE Drilling & Completion* **25** (03): 314-321. https://doi.org/10.2118/97347-PA.

Nelson, E. B. and Barlet-Gouédard, V. 2006. Thermal Cements. In *Well Cementing*, ed. E. B. Nelson and Dominique Guillot, Chap. 10, 319-341. Sugarland, Texas: Schlumberger.

Nelson, E. B., Drochon, B, Michaux, Michel et al. 2006. Special Cement Systems. In *Well Cementing*, ed. E. B. Nelson and Dominique Guillot, Chap. 7, 233-268. Sugarland, Texas: Schlumberger.

Nelson, E. B. and Michaux, Michel. 2006. *Chemistry and Characterization of Portland Cement*. Sugar Land, Texas: Schlumberger.

NORSOK. 2013. NORSOK Standard D-010, Well Integrity in Drilling and Well Operations. Report No. Rev. 4, Standards Norway, Norway (June 2013).

NPC. 2011. *Plugging and Abandonment of Oil and Gas Wells*: Working Document of the NPC North American Resource Development Study (Reprint). https://www.npc.org/Prudent_Development-Topic_Papers/2-25_Well_Plugging_and_Abandonment_Paper.pdf.

Oil & Gas UK. 2015. *Guidelines on qualification of materials for the abandonment of wells, Issue 2*. Great Britain: Oil & Gas UK.

Oil & Gas UK. 2016. Decommissioning Insight 2016. Report No. UP003, (2016).

Opedal, N., Cerasi, Pierre, and Vralstad, Torbjorn. 2019. Cement Bond Strength Measurements. *Proc.,* 38th International Conference on Ocean, Offshore and Arctic Engineering OMAE2019, Glasgow, Scotland, UK.

Patchen, F. D. 1960. *Reaction and Properties of Silica-Portland Cement Mixtures Cured at Elevated Temperatures*, Society of Petroleum Engineers (Reprint). https://doi.org/.

Powers, T. C. 1958. Structure and Physical Properties of Hardened Portland Cement Paste. **41** (1): 1-6. https://ceramics.onlinelibrary.wiley.com/doi/abs/10.1111/j.1151-2916.1958.tb13494.x.

Reddy, B. R., Xu, Ying, Ravi, Kris et al. 2009. Cement Shrinkage Measurement in Oilwell

Cementing--A Comparative Study of Laboratory Methods and Procedures. *SPE Drilling & Completion* **24** (01): 104-114. https://doi.org/10.2118/103610-PA.

Scott, James B. and Brace, Robert L. 1966. Coated Casing-"A Technique for Improved Cement Bonding ". *Proc.,* Drilling and Production Practice, 1966-01-01.

Siemens PLM Software. 2017. *Star-CCM+* (Reprint). https://mdx.plm.automation.siemens.com/star-ccm-plus.

Skorpa, Ragnhild and Vrålstad, Torbjørn. 2018. Visualization of Fluid Flow Through Cracks and Microannuli in Cement Sheaths. *SPE Journal* **23** (04): 1,067-1,074.

Smith, Ian and Shu, Dominique. 2013. A Strategic Shift in Well Abandonment Services. *Oil and Gas Facilities* **2** (01): 19-21. https://doi.org/10.2118/0213-0019-OGF.

Stormont, John C., Fernandez, Serafin Garcia, Taha, Mahmoud R. et al. 2018. Gas flow through cement-casing microannuli under varying stress conditions. *Geomechanics for Energy and the Environment* **13**: 1-13. http://www.sciencedirect.com/science/article/pii/S2352380817300436.

Therond, Emmanuel, Bois, Axel-Pierre, Whaley, Kevin et al. 2017. Large-Scale Testing and Modeling for Cement Zonal Isolation in Water-Injection Wells (in english). *SPE Drilling & Completion* **32** (04): 290-300.

Thiercelin, M. 2006. Mechanical Properties of Well Cements. In *Well Cementing*, ed. E. B. Nelson and Dominique Guillot, Chap. 8, 269-288. Sugar Land, Texas: Schlumberger.

Trudel, E., Bizhani, M., Zare, M. et al. 2019. Plug and abandonment practices and trends: A British Columbia perspective. *Journal of Petroleum Science and Engineering* **183**: 106417. http://www.sciencedirect.com/science/article/pii/S0920410519308381.

van Eijden, Jip, Cornelissen, Erik, Ruckert, Frank et al. 2017. Development of Experimental Equipment and Procedures to Evaluate Zonal Isolation and Well Abandonment Materials. *Proc.,* SPE/IADC Drilling Conference and Exhibition, March 14-16, 2017.

Vrålstad, Torbjørn, Saasen, Arild, Fjær, Erling et al. 2019. Plug & abandonment of offshore wells: Ensuring long-term well integrity and cost-efficiency. *Journal of Petroleum Science and Engineering* **173**: 478-491. http://www.sciencedirect.com/science/article/pii/S0920410518309173.

Zeng, Zhengwen and Grigg, Reid. 2006. A Criterion for Non-Darcy Flow in Porous Media. *Transport in Porous Media* **63** (1): 57-69. https://doi.org/10.1007/s11242-005-2720-3.

Zhang, Wenhua, Zhang, Yunsheng, Liu, Laibao et al. 2012. Investigation of the influence of curing temperature and silica fume content on setting and hardening process of the blended cement paste by an improved ultrasonic apparatus. *Construction and Building Materials* **33**: 32-40. http://www.sciencedirect.com/science/article/pii/S0950061812000347.

Zou, Liangchao, Jing, Lanru, and Cvetkovic, Vladimir. 2017. Shear-enhanced nonlinear flow in rough-walled rock fractures. *International Journal of Rock Mechanics and Mining Sciences* **97**: 33-45. http://www.sciencedirect.com/science/article/pii/S1365160917306810.

Appendix A
Supplementary materials for Chapter 5

A.1. Sensitivity analysis of models for the CFD simulation

A sensitivity analysis was conducted to examine the suitable geometry of leak path models that are accurate in output without requiring excessive CPU time. By using the representative of a leak path model with moderate roughness, two geometries with different length – i.e. 10.3 cm and 4.9 cm – and five geometries (Fig. A. 1) with different degrees of simplification were prepared.

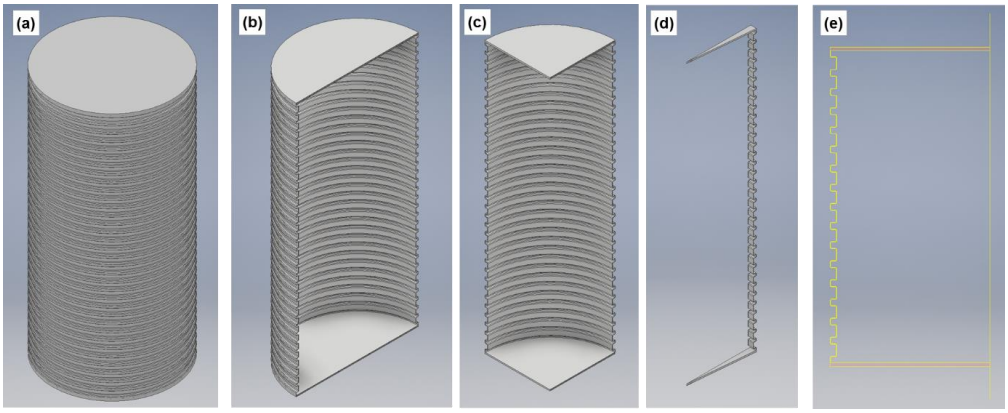

Fig. A. 1. Five leak path geometries with different degree of simplifications for sensitivity analysis: (a) 3D, (b) half-symmetry, (c) quarter-symmetry, (d) 5 degree rotational-symmetry, and (e) 2D axisymmetric

Results showed that the simpler and the shorter the geometries, the less CPU time was required. Results also showed that the output of mass flow rate was not sensitive to change in the model length, but sensitive to change in geometry simplification, as indicated in Table A. 1 and Table A. 2. Based on these results, the leak path models used in each simulation objective are described as follows:

- the estimation of microannuli width would be run using the model with the simplification of 5-degree rotational symmetry and length of 4.9 cm, and
- the fluid flow visualization would be run using the model with the full-3D and length of 10.3 cm.

Table A. 1. Results of sensitivity analysis from different leak path lengths (microannuli width = 0.1 mm), run at $\nabla P = 0.48$ bar/m

Geometry length	Mass flow rate (kg/s)	Difference (%)[†]
10.3 cm	3.0145×10^{-3}	-
4.9 cm	3.0151×10^{-3}	0.02

[†)] The difference in mass flow rate was calculated based on the output from geometry length of 10.3 cm

Table A. 2. Results of sensitivity analysis from different geometries (microannuli width = 0.1 mm and length = 4.9 cm), run at $\nabla P = 0.48$ bar/m

Geometry	Mass flow rate (kg/s)	Difference (%)†
Full 3D (10.3 cm)	3.0145 x 10^{-3}	-
Half-symmetry	3.0151 x 10^{-3}	0.02
Quarter-symmetry	3.0074 x 10^{-3}	0.24
5 degree rotational-symmetry	3.0624 x 10^{-3}	1.6
2D axisymmetric	2.9063 x 10^{-3}	3.5

†) The difference in mass flow rate was calculated based on the output from full 3D geometry

A.2. Simulation results: effect of uniform microannulus surface roughness to fluid dynamic at the condition of 120° C

This chapter presents the results of CFD simulation from microannulus with smooth and high-rough surfaces run at T=120° C (relevant for test results of silica cement system). The uniform microannulus apertures that were equivalent to the averaged leak rate found from the silica cements are summarized in Table A. 3. The plot between the pressure gradient and flow rate from the simulation results compared to the experimental results of the silica cement plug is shown in Fig. A. 2.

Table A. 3. Summary of the equivalent microannulus width based on experimental results of silica cement

Test pipes	Equivalent microannuli width*)
Smooth	14 μm
High rough	7.4 μm

*) *The presented value has a 1-digit of decimal precision to produce a mass flow rate with <1% deviation*

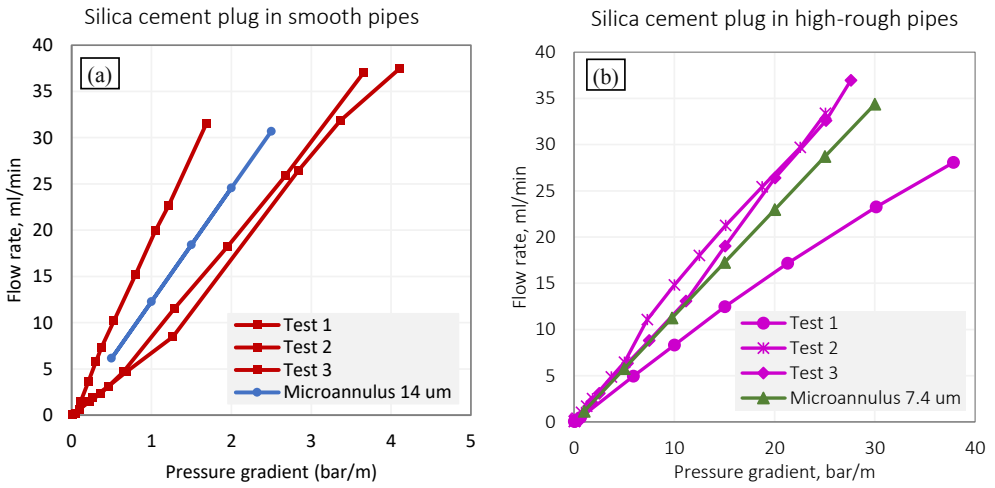

Fig. A. 2. Plots of ∇P vs. Q from the experimental test of silica cement systems (T=120° C), plotted together with uniform microannulus results from the fluid dynamics simulation

Table A. 4. Summary of mass flow rates through microannuli (width=0.1 mm) with different roughness computed from the fluid simulation at a differential pressure of 1 bar and temperature 120° C

Leak path models	Mass flow rate (kg/s)
Smooth	1.1 x 10^{-2}
High rough	3.4x 10^{-3}

Appendix B

Paper I

Nils Opedal, Anisa Noor Corina, Torbjørn Vrålstad

Laboratory Test on Cement Plug Integrity

This paper was presented at ASME 2018 37th International Conference on Ocean, Offshore and Arctic Engineering in Madrid, June 2018 and published in the conference proceedings. doi: 10.1115/OMAE2018-78347.

Proceedings of the ASME 2018 37th International Conference on Ocean, Offshore and Arctic Engineering
OMAE2018
June 17-22, 2018, Madrid, Spain

OMAE2018-78347

LABORATORY TEST ON CEMENT PLUG INTEGRITY

Nils Opedal
SINTEF
Trondheim, Norway

Anisa Noor Corina
Norwegian University of Science & Technology
Trondheim, Norway

Torbjørn Vrålstad
SINTEF
Trondheim, Norway

ABSTRACT

A recurring issue in the petroleum industry is the performance of cement in relation to its primary role of providing zonal isolation. Enhanced understanding of this subject offers the possibility to improve the planning and design of the cementing job to minimizing the risk of poor bonding of cement and loss of well integrity. The design and execution of the cement job is by no means an easy task, mainly due to the complexity of the material and process, and the variety in conditions one can encounter downhole. Thus, screening of different materials and conditions is necessary to optimize the success of a cement operation.

This work focused on experimentally testing cement plugs to be able to understand the sealing ability of cement to a casing at relevant temperatures and pressures. A built-for-purpose test setup was designed and assembled, and the goal of this work was to test this new setup and to establish a proper baseline for future test on various cement systems.

The setup consists of a test cell containing the cement plug, an automated pressure regulator used for generating a pressure differential across the cement plug and flow meters to measure the flow rate through the cement plug. The output data from the tests is the differential pressure needed to have breakthrough of gas, and the connection between the flow rate and differential pressure across the cement plug. The possible manipulated variables for the test setup is the cement type and casing surface properties.

INTRODUCTION

Due to the high cost of having a non-successful well cementing operation, it is important to be properly prepared. The complexity of the job itself can be imaged by all the possible parameters involved, such as the temperature and pressure in the well, the complex cement chemistry and interplay with drilling fluids and/or rock formations. As many as possible unknowns should be mapped in order to minimize the risk of failure. Models can be a valuable tool for risk mitigation. However, a central part of any model is access to data from experimental tests performed at wellbore relevant conditions.

Various dedicated test setups for investigating the performance of *cement slurries* have been designed and presented. The tests setups can vary from established small-scale setups dedicated for effects such as cement slurry shrinkage [1] or thickening time [2] to unique large-scale custom-built setups to study displacement of drilling fluids [3].

In relation to setups used to study the properties of *cured cement,* the reader can also find a variety of complexities in the design. Measurements of cement compressive strength [4], or tensile strength [5] are established techniques. Various small-scale setups have also been made to study effects such as shear bond [6-8] or tensile bond strength [9,10] of cement. Values on the bond strength for a specific case, either the shear bond or tensile bond is an important input for comparison and optimization of a cement system for a given application, but are also valuable input for the fundamental understanding of the system.

The ability to provide zonal isolation is perhaps the most important role of cement in the well. Both the *Guidelines on qualification of materials for the suspension and abandonment of wells* by the Oil & Gas UK [11], and *Well integrity in drilling and well operations* by the NORSOK standard [12] outline the importance of the ability of a cement plug in relation to petroleum operations. The compressive, tensile, shear bond or tensile bond strength do not give a direct measure of the ability of a material to provide zonal isolation. To obtain a measure of the level of zonal isolation, a purpose-built setup that actually *measures* the flow rate through the

sample is needed. Carter and Evans [6] performed numerous lab-scale test on the hydraulic bond strength between various cement systems to pipes and rock formations. On the other hand, Wilson and Sabins [3] performed full-scale displacement and cementing tests and performed hydraulic bond strength tests on their samples. Van Eijden et al [13] described two setups, one small scale and one large-scale, both built for the purpose of qualitatively ranking cementitious systems for Plug & Abandonment operations. Due to the nature of their design, with pressure applied vertically across the cement plug, these two setups are actually applying/measuring both shear bond and hydraulic bond strength at the same time. Nonetheless, both setups provide valuable and relevant data.

In this work, we present the preliminary results of a cement plug test setup designed and built with the purpose of investigating the parameters relevant for the sealing ability of a cement system. The design of the setup has been based on the one described by van Eijden et al [13] and also by Oil & Gas UK [11]. Potential relevant parameters that could be studied are the pipe surface properties or the properties of the cement system itself. The setup has the following design features:

- Cure cement under temperature and pressure
- Avoid evacuation of cement plug (test specimen) between curing and experimental testing
- Measure gas flow rate to quantify leakage rate
- Measure minimum differential pressure before cement plug fails.
- Differential pressure obtained by reduction on one side to avoid ballooning of test cell
- Automated test procedure to minimize effect of human factors

MATERIALS AND METHODS

Materials

Smooth steel pipes were used as test sections. The cement used in the experiments was Portland G provide by NORCEM AS. The cement paste was prepared according to API standard 10b with no additives and with a water-to-cement ratio of 0.44. Industrial grade Nitrogen gas was used to pressurize the system.

Cement plug integrity test setup

The setup consists of a custom-built test cell containing the cement plug placed inside a heating cabinet for temperature control, and a process board located outside the heating cabinet with the process tubing, valves, flow meters, pressure indicators, an automated pressure regulator and an automated logging system. A sketch of the test cell is shown in figure 1. The major components of the test cell is:

- Bottom cap with two Swagelok 1/8 " connection ports and a built-in movable teflon piston used for retaining the cement slurry during curing.
- Expandable steel pipe with inner diameter of 50 mm, wall thickness of 13 mm and a length allowing a maximum of 460 mm of cement to be placed inside the pipe.
- Top cap with two Swagelok 1/8 " connection ports.

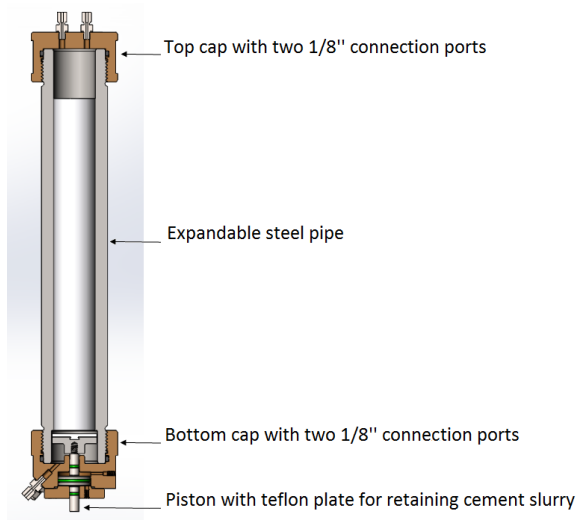

Figure 1 Sketch of test cell.

A technical drawing of the cell is shown in figure 1. A pressure test at 100 bar and 22 °C was performed on the test cell showing no signs of deformation on pipe diameter or damage to the pipe threads.

Figure 2 Photographs of test cell. Top left: bottom cap with tefon piston removed. Top right: teflon piston. Bottom left: bottom cap with teflon piston mounted. Bottom right: Fully assembled test setup inside heating cabinet.

Figure 2 shows a collection of photographs of the test cell. The teflon plate used to retain the cement slurry during curing is

slided onto a rail on a steel disk. The combined teflon/steel disk is then screwed onto the vertically moving piston. An automated pneumatic unit moves the piston up and down.

Figure 3 shows a simplified P&ID of the setup, which consists of:

- A manual pressure regulator (item R101) to control the pressure to the setup
- An automated pressure regulator (item R102) used for generating a pressure differential across the cement plug
- Two Bronkhorst Mass Flow Meters (VF1 measure range 0-50 mL/min, VF2 measure range 0-500 mL/min) to measure the flow rate through the cement plug
- Two GE-Druck pressure indicators (PI)
- One Fuji Electric FCX pressure transmitter (dP)

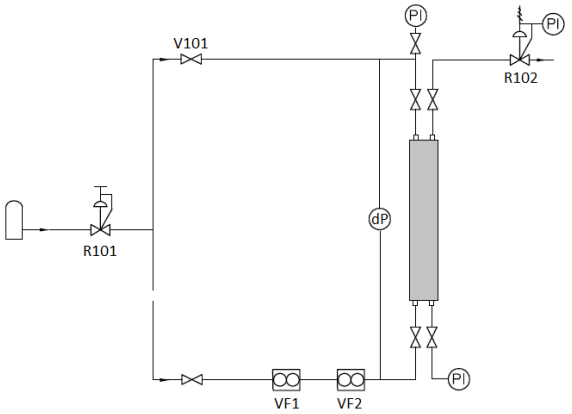

Figure 3 Simplified P&ID of test setup showing the most important elements.

The test setup is also equipped with a temperature probe for control of the experimental conditions. The output data from the tests is the differential pressure needed to observe breakthrough of gas through the cement plug, and the relationship between the measured flow rate and differential pressure across the cement plug. Possible manipulated variables for the test setup can be the cement type and casing surface properties.

Procedure for testing.

Before every new experiment, a pressure test was performed on every new test cell. This was done by fully mounting the test setup with no cement inside the cell. The setup would then be pressured up to the working pressure (20 bar) and the main valve to the pressure bottle would be closed. By monitoring the decrease in pressure over a period of 1-2 hours, the level of gas leakage from the entire setup was monitored. In an ideal situation there would be zero leakage; in a case of losing more the ~1 bar over 1 hour an attempt to localize the leakage would be performed. If the pressure test was assessed to be successful the gas in the setup would be evacuated and the top cap to the test cell would be unscrewed.

The cement placement was performed by moving the teflon piston in its top-position and by pouring the designated cement volume into the test cell. All valves would be opened and the automated pressure regulator (item R102 in figure 3) would be set to maintain a minimum pressure of 20 bar. The top cap would be screwed in place tightly and the cell would be carefully pressurized to 20 bar. The cement plug would be left to cure at 20 bar and 66 °C for 5 days.

The cement plug integrity test started by moving the teflon piston down, leading to an open volume above and below the cement plug. By closing valve V101 (shown in figure 3) these two chambers would be isolated from each other and the only connection between them could be through the cement plug. By using the automated pressure regulator (item R102 in figure 3) a controlled differential pressure across the cement plug was generated. When the differential pressure was large enough for enabling flow through the cement plug, the pressure regulator connected to the bottom chamber (item R101 in figure 1) would detect a decrease in pressure, and the regulator would try to maintain the set pressure. This flow of gas from the gas bottle through the process line would be detected by the flow meters. A sequential increase in the differential pressure would be applied to the cement plug. Thus, each experiment gives the pressure differential to which there is gas breakthrough the cement plug, and the relationship between the applied differential pressure and the flow rate through the cement plug.

RESULTS & DISCUSSION

The primary objective of the first three experiments was to obtain a proper reproducible baseline for future studies where a variety of parameters can be compared. *The baseline was in this study defined as a cement system of Portland cement Class G with no additives*. The baseline tests were performed with three parallels by curing a 40 cm "dry" (i.e. no access to extra water during curing) cement column inside the test cell and by carefully applying a sequential increase in the differential pressure across the cement plug. Figure 4 shows the result from one of the baseline experiments. The blue diamonds show the applied differential pressure in bar, and the orange lines show the measured flow rate in mL/min through the cement plug. This kind of cement system exhibited measured flow through the cement plug at a differential pressure of ~0.04 bar, a reproducible value for all three parallels. As seen in the plot the relationship between the applied differential pressure and the measured flow rate follows in a linear manner.

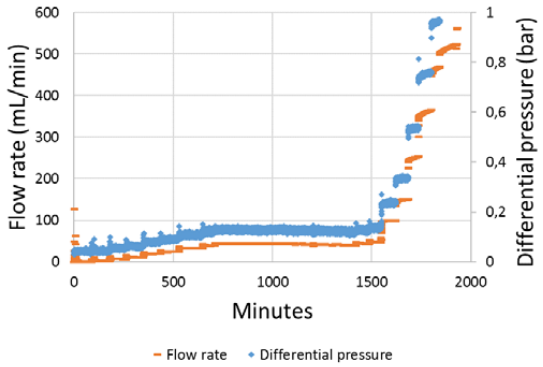

Figure 4 Example of a result from a baseline experiment with a "dry" 40 cm cement column.

By combining the relationship between the applied differential pressure and the measured flow rate for all three parallels, one can assess the level of reproducibility for these kinds of experiments. Figure 5 shows this comparison for the three experiments, and as seen, the linear relationship follows the same trendline for all three parallels. The first parallel is missing measurements of flow rate exceeding 56 mL/min due measurement errors with the high-range flow meter. Nevertheless, the similarities in the behaviour between the second and third parallel at higher flow rates/differential pressures is relatively promising.

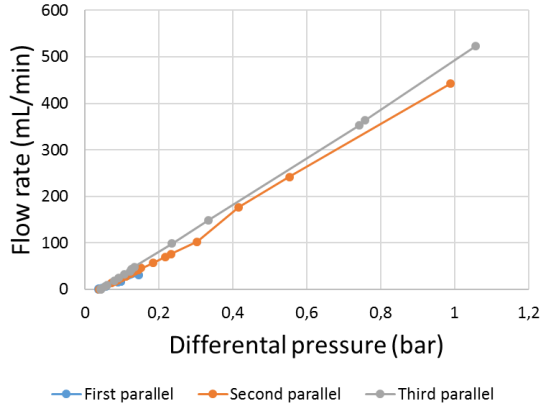

Figure 5 Relationship between applied differential pressure and measure flow rate for all three baseline experiments.

To further investigate the behaviour of cement in the test setup, it was decided to prepare similar cement plugs, but with access to water during the curing. The main reason for this was the relatively low differential pressure needed to initiate flow through the cement plugs for the first three parallels. This was done by preparing the cement plug in the same manner as described above, but to place water on top of the cement slurry before closing the top cap and curing and testing under pressure. Due to the availability of water (therefore named wet" experiments) to the cement slurry during curing it was assumed that the volumetric shrinkage would be reduced, and the reduce shrinkage would mean a higher differential pressure would be needed to initiate flow through the cement plug. Figure 6 shows the result from such an experiment were a 40 cm cement column was placed with 4 cm of water on top of the cement. As one can see from the measured flow rate, this kind of cement plug exhibited more resistance to flow. No flow was detected until the differential pressure had increased to 10 bar, and the measured flow rate at the highest differential pressure (20 bar) was in the order of 1 – 1.5 mL/min.

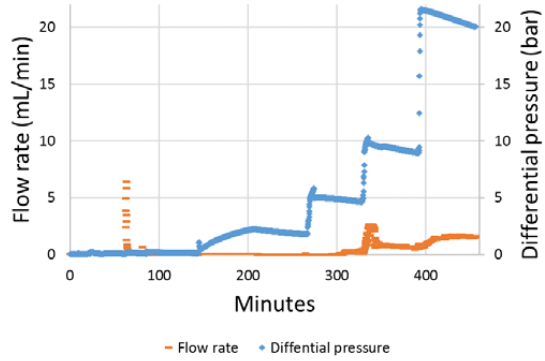

Figure 6 Result from an experiment with a 40 cm cement plug with 4 cm of water on top.

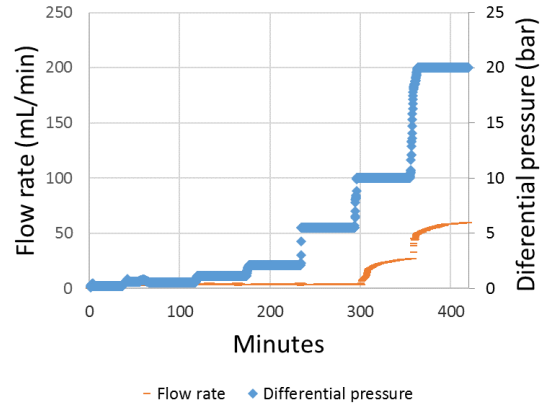

Figure 7 Result from an experiment with a 26 cm cement plug with 13 cm of water on top.

Figure 7 shows the results from a similar test. This particular cement plug was 26 cm of length with a 13 cm column of water on top of the cement during curing and testing. This test did not exhibit gas breakthrough until a differential pressure of 10 bar was applied. By comparing the flow rates for the two "wet" experiments, one can see that the shorter cement plug exhibits higher flow rates at similar differential pressure. The 26 cm cement column (figure 7) has a flow rate close to 60 mL/min at 20 bar differential pressure, whereas the 40 cm cement column had a flow rate of 1.5 mL/min. The length is a natural and expected factor for describing these kind of test results. However, since no information on the flow paths given in this study it is difficult to compare the flow rates for the "wet" experiments due to the capillary effects of water inside the cracks/leakage paths.

CONCLUSION

A test setup with the purpose of investigating the sealing ability of cement to steel pipe have been built and tested. The preliminary study focused on obtaining a good and reproducible baseline, and the setup has been found to be operational. The baseline experiments were defined as dry experiments with Portland G cement with no additives, and they gave a reproducible gas breakthrough pressure of 0.04 bar with the flow rate increasing linearly with the applied differential pressure. Experiments with a water column on top of the cement column gave breakthrough at a higher pressure (10 bar). However, the presence of water in the test section makes it difficult to separate between crack propagation through cement-steel interface and capillary effects of water in capillaries.

The setup is able to give relevant data for qualitative comparison of different cement systems. It can also be used to study the effect of pipe surface properties such as surface roughness or level of rust.

ACKNOWLEDGMENTS

The authors are grateful for the financial support for this work granted through The Drilling and Well Centre for Improved Recovery (DrillWell), which is funded by the Research Council of Norway, Aker BP, ConocoPhillips, Statoil and Wintershall.

REFERENCES

[1] Justnes H. van Loo D. Reyniers B. Skalle P. Sveen J. Sellevord E. J. "Chemical shrinkage of oil well cement slurries". *Advances in Cement Research* Vol. 7 No 26 (1995): pp 85-90. DOI 10.1680/adcr.1995.7.26.85

[2] McElfresh, Paul and Cobb, Jo Ann. "Chemical Thickening-Time Test for Cement Blends". *Journal of Petroleum Engineers* Vol 35 No 02 (1983). DOI 10.2118/10220-PA.

[3] Wilson M.A. Sabins, Fred. "A Laboratory Investigation of Cementing Horizontal Wells". *SPE Drilling Engineering* Vol 3 No 03. DOI 10.2118/16928-PA

[4] Sabins, Fred and Sutton, David. "The Relationship of Thickening Time, Gel Strength, and Compressive Strength of Oilwell Cements". *SPE Production Engineering* Vol 1 No 02 (1986). DOI 10.2118/11205-PA

[5] Bybee, Karen. "Analysis of Tensile-Strength Test Methods for Oilfield Cement". *Journal of Petroleum Technology* Vol 56 No 08 (2004). DOI 10.2118/0804-0062-JPT.

[6] Carter L.G. Evans G.W. "A Study of Cement-Pipe Bonding". *Journal of Petroleum Engineers* Vol 16 No 02 (1964) DOI 10.2118/764-PA

[7] Opedal, Nils, Torsæter, Malin, Vrålstad, Torbjørn, Mushtaq, Waqas. "Experimental Study on the Cement-Formation Bonding". *SPE International Symposium and Exhibition on Formation Damage Control* SPE 168138-MS. Lafayette, LA, 2014. DOI 10.2118/168138-MS.

[8] Ladva, Hemant, Craster, Bernadette, Jones, Timothy, Goldsmith Garry, Scott, David. "The Cement-to-Formation Interface in Zonal Isolation. *SPE Drilling & Completion* Volume 20 No 03 (2005). DOI 10.2118/88016-PA

[9] Lavrov, Alexandre, Gawel, Kamila, Stroisz, Anna, Torsæter, Malin, Bakheim, Sigurd. "Failure modes in three-point bending tests of cement-steel, cement-cement and cement-sandstone bi-material beams". *Construction and Building Materials* Vol 152 (2017): pp880-886. DOI 10.1016/j.conbuildmat.2017.07.017.s

[10] Lummer, N. Block, R. Yadigarov, Y. "Specially Customized Systems for Cementing Glass Reinforced Epoxy GRE Casings – Development and Field Trials in a Geothermal Project". *SPE/IADC Drilling Conference and Exhibition* SPE-184597-MS, den Haag, the Netherlands, 2017. DOI 10.2118/184597-MS.

[11] The United Kingdom Offshore Oil and Gas Industry Association Limited. (Oil & Gas UK). "Guidelines on qualification of materials for the suspension and abandonment of wells". London (2015). Issue 2.

[12] Standards Norway. "Well integrity in drilling and well operations". NORSOK standard D-010. 2013. Rev. 4.

[13] van Eijden, Jip. Cornelissen, Erik. Ruckert, Frank and Wolterbeek, Tim. "Development of Experimental Equipment and Procedure to Evaluate Zonal Isolation and Well Abandonment Materials". *SPE/IADC Drilling Conference and Exhibition* SPE-184640-MS, den Haag, the Netherlands, 2017. DOI 10.2118/184640-MS.

Appendix C

Paper II

Anisa Noor Corina, Nils Opedal, Torbjørn Vrålstad, Sigbjørn Sangesland

Cement Plug Sealing Studies of Silica Cement Systems

This paper was presented at ASME 2019 38th International Conference on Ocean, Offshore and Arctic Engineering in Glasgow, June 2019 and published in the conference proceedings. https://doi.org/10.1115/OMAE2019-95928.

Proceedings of the ASME 2019 38th International Conference on Ocean, Offshore and Arctic Engineering
OMAE2019
June 9-14, 2019, Glasgow, Scotland

OMAE2019-95928

CEMENT PLUG SEALING STUDIES OF SILICA CEMENT SYSTEMS

Anisa Noor Corina
Norwegian University of Science and Technology
Trondheim, Norway

Nils van der Tuuk Opedal
SINTEF
Trondheim, Norway

Torbjørn Vrålstad
SINTEF
Trondheim, Norway

Sigbjørn Sangesland
Norwegian University of Science and Technology
Trondheim, Norway

ABSTRACT

A cement plug is widely applied for permanent abandonment phase to provide long-term zonal isolation against fluid flow. Maintaining cement plug integrity is a challenging task, and loss in cement sealing poses risks to the surrounding environment and surface safety. It is well-known that the cement performance is affected by cement material and downhole conditions. Nevertheless, investigations linking these influencing factors with the sealing of cement plugs are still limited, especially with the lack of proper equipment in the past.

In the present work, a small-scale laboratory setup has been constructed to test the sealing ability of a cement plug. It has unique features that can simulate plugging operations at the downhole conditions and preserve the cement curing condition. By testing using this setup, it is possible to measure the minimum differential pressure required for gas to flow across the cement plug and the gas leak rate. The silica cement mixture was selected as the plug material, prepared using silica flour. Investigation of silica cement under the influence of expanding agent additive and various curing temperature was carried out. It was found that adding an expanding agent improved the sealing of cement plugs. Moreover, samples cured at a high temperature were less resistant to gas flow with the leak path observed at the cement/steel interface, indicating debonding.

INTRODUCTION

In well abandonment phase, the wellbore shall be plugged using materials that are sufficient to isolate a source of inflow from the surrounding formation. For a permanent application, the plugging materials shall provide integrity that lasts for an eternal perspective [1, 2]. Among those materials, Portland cement is the most common sealant material for plug-and-abandonment (P&A) operations, although several case studies show that the cement-plug system fail to provide a tight seal due to issues related to cement placement and behavior [3, 4]. Furthermore, conventional Portland cement systems deteriorate when placed in wells with elevated temperature causing strength retrogression and increase in permeability [5, 6]. This condition can escalate the risk of cement to lose its sealing ability, failing to provide the required integrity of P&A wells.

One of the solutions to prevent strength retrogression at elevated temperatures is the addition of silica. Silica is one type of pozzolans that comes in forms of (a) crystalline phase, such as silica sand and silica flour, and (b) amorphous phase, such as condensed silica fume (microsilica). Early research showed the set cement that was mixed with silica has high compressive strength and very low water permeability even when cured at elevated temperature, even less than 0.01 mD [5–9]. Aside from this, a study found that the silica mixed cement produced better bonding than the conventional cement system, especially at elevated temperature greater than 120^{o} C [10]. These past studies measuring different properties of the silica cement presented valuable insight. However, a different approach was required to fully understand the sealing performance of cement placed inside the casing (cement plug) as a single system.

New approaches to laboratory evaluation of cement plug sealing have been proposed and developed in recent years [11, 12]. In this study, we used a small-scale laboratory setup which was based on the one described by van Eijden et al. [12] and also by Oil & Gas UK Guidelines [13]. Using the following setup, the sealing function of plug made of different cement systems can be evaluated and compared qualitatively. External factors, such as pipe roughness, or curing condition, could also be studied. The setup was designed to mimic the cement plug operation, including cement placement and cement curing. It can preserve the curing condition systematically while testing the plug to prevent alteration of cement and casing properties. The concept of the test is applying differential pressure across the cement

plug. As the results, we can obtain the value of breakthrough pressure, i.e. the smallest differential pressure required for gas to fully flow across the cement plug. The setup is also equipped with gas flowmeters, and hence the gas leak rate through the cement plug can be measured once it fails to seal. Our previous studies have confirmed the conductibility of the setup and reproducibility of the test results [14, 15].

The current study is an extension of our previous work, which specifically focused on silica cement system made of silica flour. The objective of this study is to look into the effect of various downhole temperature. Another aspect that was investigated is the effect of additive of expanding agent on the sealing of cement plug.

EXPERIMENTAL SETUP AND PROCEDURE

Setup description

The small-scale laboratory setup used in the present work is presented in Figure 1. It contained a test cell for holding a cement plug sample, placed inside a heating cabinet. This test cell was connected to a pressurizing system, flowmeters, and an automated logging system. Accordingly, the setup could be operated at elevated temperature and pressure resembling the downhole condition. The pressure system was equipped with nitrogen feed and pressure regulators for control.

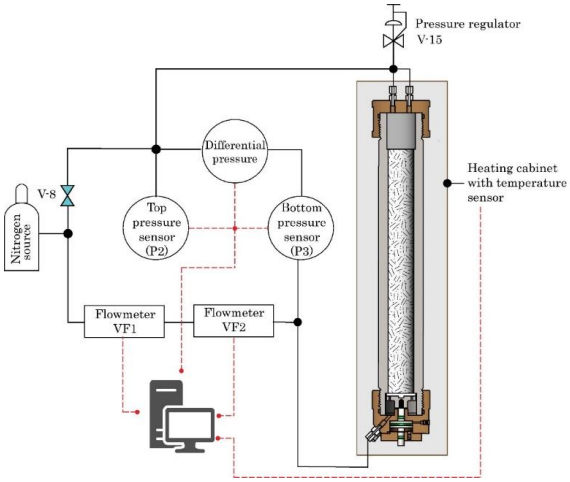

Figure 1. A simplified diagram of important elements of the setup [15]

A schematic of the test cell is shown in Figure 2. Both ends of the test cell were enclosed by removable caps with gas inlets. The bottom cap is mounted with an adjustable support system for retaining the liquid phase of the cement slurry during curing. This support system contained two elements: (1) a Teflon plate, to prevent adhesion with cement, and (2) a piston, to regulate the position of the system. It was placed upward during the curing process, providing support when the cement was still in liquid

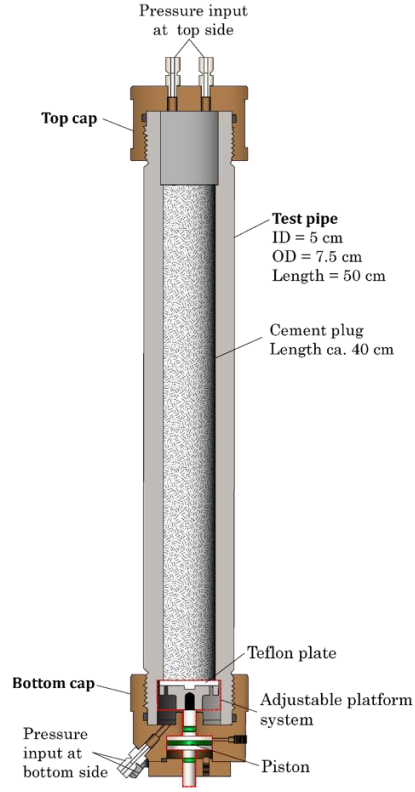

Figure 2. Schematic of small-scale setup with features of adjustable platform system [15]

form. After the cement cured, the support system was placed in a downward position, and the cement could be tested using the same setup.

Test procedure and outputs

Prior curing, the setup was checked for leak and preheated to the desired temperature. Then, the cement slurry was poured by gravity into the test cell and cured under certain pressure and temperature until cement set. Before conducting the test, valve V-8 (see Figure 1) was closed to create a bypass line for gas to flow through the test cell. Subsequently, two pressure lines, on the top- and bottom sides of the test cell, could be regulated separately.

Afterward, the pressure at the top side of the test cell was reduced while the pressure at the bottom side of the test was kept constant. Therefore, a pressure drop was created across the cement plug. Once the pressure reading stabilized, the test was monitored for 1-2 hours. The first gas leak detected in the flowmeter reading indicated that the cement plug has failed. In this case, the test was maintained until the gas flow rate stabilized or reached the steady-state flow. And then, these processes were

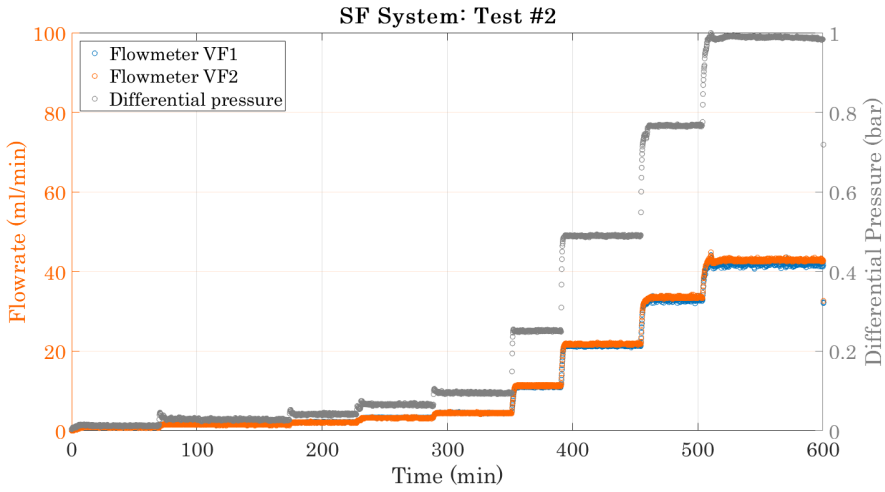

Figure 3. Example of reading from flowmeters and pressure sensors during the test plotted against time

Table 1. Curing condition of tested cement systems

Cement system	Cement composition			Curing condition		
	Water (% BWOC)	Silica flour (% BWOC)	Expanding agent (% BWOC)	Pressure (bar)	Temperature (ºC)	Curing period (days)
SF-66	62	35	-	20	66	4
SF-120 [15]	62	35	-	20	120	4
SF -120 + EA	62	35	2	20	120	4

repeated by decreasing the top pressure even further, consequently increasing the differential pressure, until it reached atmospheric pressure or until the flowmeters reached their maximum reading.

The typical reading of differential pressure and gas flow rate during the test is shown in Figure 3. Then, the flow rate data was corrected to the pressure and temperature test, see Annex A. These data were extracted to gain following information: (a) the breakthrough pressure and (b) the relationship between gas leak rate and differential pressure.

SAMPLE PREPARATION

Cement systems

The cement type used for the current study was Class G Portland cement, provided by NORCEM AS. The form of silica added in the cement system is silica flour, which is a crystalline-silica (α-quartz) that has an average particle size of 15 µm and specific surface of 0.4 m^2/g [8]. It has a form of dry white powder.

Three silica cement systems were prepared with 62% BWOC of water and 35% BWOC of silica flour, whereas 2% expanding agent was added to one of the mixture (see Table 1). One of the experiments was extracted from past study [15]. They were mixed following API RP 10B-2 [16] and then poured into test cell pipe. They were cured for a four-day period under pressure of 20 bar and two different temperatures (66º C and 120º C), as seen in Table 1. All samples were dry cured with no external water source.

Pipe material

Pipes of the test cell were made of steel material with no coating. The roughness of pipes was measured as parameter Ra by using MarSurf PS 10 (see Annex B for more details). The averaged Ra of all pipes is ranging from 2-5 µm.

EXPERIMENTAL RESULTS

To improve the result accuracy, at least three samples from each experimental cases must produce results with similar trends. Results from the test were presented as a relationship between flowrate versus pressure drop across the plug, as seen in Figure 4-6.

No breakthrough pressure was observed in the samples of SF-66 and SF-120. This was indicated by an immediate gas leak in the plugs just after the bypass line through the test cell was opened. At this period, the applied differential pressure was very low, which was less than 0.01 bar, and hence it could be neglected. The occurrence of no-breakthrough pressure was an indication that there was a significant leak path formed in all of these samples.

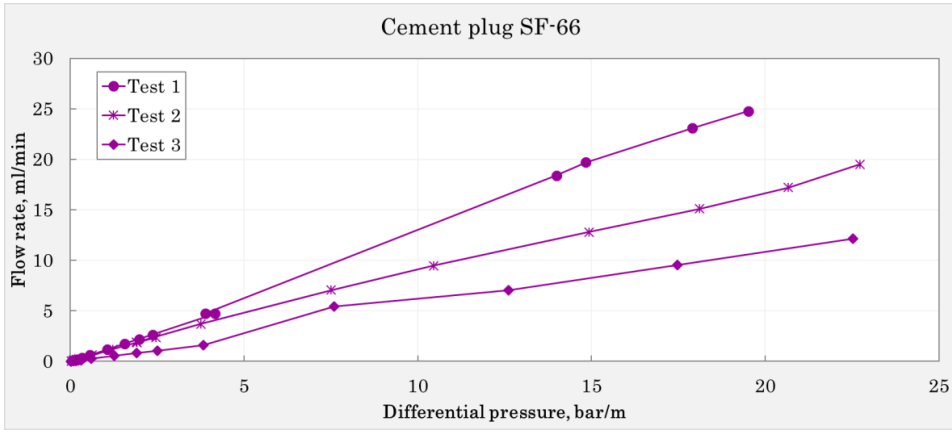

Figure 4. Curve of flow rate plotted against differential pressure from samples of SF-66 system

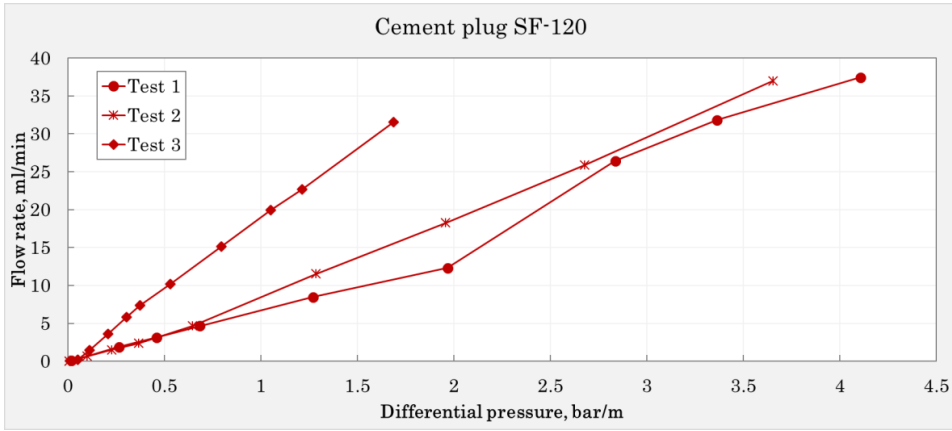

Figure 5. Curve of flow rate plotted against differential pressure from samples SF-120 system [15]

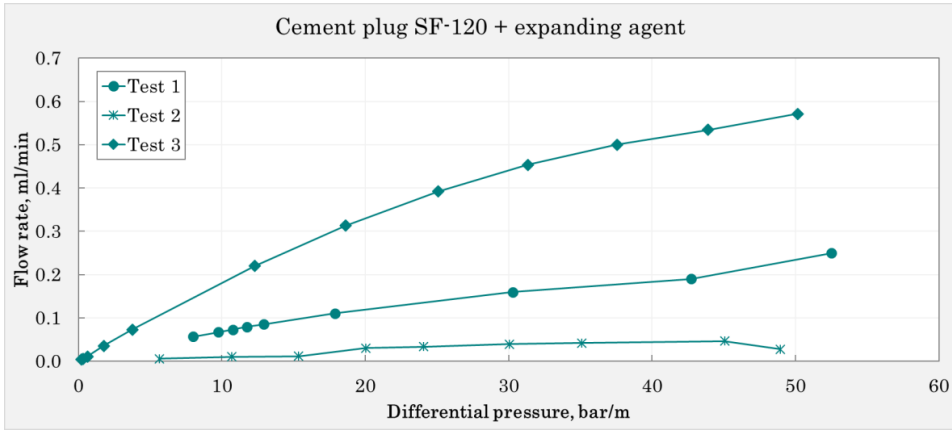

Figure 6. Curve of flow rate plotted against differential pressure from samples SF-120 + EA

On the other hand, breakthrough pressure was not clearly defined when testing samples of SF-120 with an expanding agent. As soon as the bypass line through test cell was opened, the top pressure decreased gradually and, simultaneously, a low leak rate was observed. The top pressure became constant after the test cell reached the differential pressure ranging from 0.03-3 bar. This behavior could be explained by the pressure difference between the setup and the cement plug. After the cement set, the pressure within the cement plug might be reduced because of the shrinkage that provokes pore contraction and dropped below the setup pressure. As a result, gas flow into the plug was observed at the beginning of the test. Because this flowing gas initially had not fully-displaced fluids within the plug, the automatic pressure regulator could not maintain a constant top pressure. The following event masking the observation of breakthrough pressure.

DISCUSSIONS

Effect of curing temperature

Results from samples cured at different temperature were plotted altogether in Figure 7. The difference of curve slope between plugs cured at different temperatures is distinct. Sharp reduction of curve slope from SF-66 samples indicates that these plugs produced smaller leak rate at each applied differential pressure compared to leak rate from SF-120 samples. At a differential pressure of 2.5 bar/m, the averaged leak rate of plugs cured at 66° C is 2.12 ml/min, which was almost ten times smaller than that of plugs cured at 120° C (22.5 ml/min).

To understand where the leak was originated, we inspected the flow source by placing a ±2 cm column of water at the top side of the plug after the test was finished. By flowing the gas from the bottom side until reaching a pressure of ±10 bar, the location of the leak path was observed from the top surface by the presence of gas bubbles in the water column. A continuous flow of gas bubbles was observed in several locations at the interface of cement plug and casing. Meanwhile, no gas bubbles was visible from the cement body after flowing gas for a long period. This observation confirmed that leak indicated in the integrity test was flowing through the leak path at the cement/casing interface instead of the cement body.

The discontinuity at the cement/casing interface was also observed in several studies [11, 17–19]. The leak path at the interface was most likely formed due to the shrinkage after the cement was hardened, or so-called autogenous shrinkage [20]. Contraction in the cement body due to shrinkage, ultimately, leads to cement to debond from steel, forming of microannuli surrounding the cement plug. This presence of microannuli in the cement plug can be critical for the well integrity because it will increase the effective permeability, even though the true permeability of the plug is small.

Increasing curing temperature accelerates the hydration and the setting time. As a result, the development rate and the amplitude of autogenous shrinkage increase rapidly at the beginning of the setting. At this early period, the shrinkage value of cement paste cured at elevated temperature is larger than that of paste cured at low temperature, even though it reduces at later age [21, 22]. Not only cement hydration, but also the pozzolan reaction rate of silica flour are highly dependent in curing temperature in a similar manner. It has been investigated that the pozzolan reaction could also intensify the system shrinkage alongside with the cement hydration [21, 23, 24].

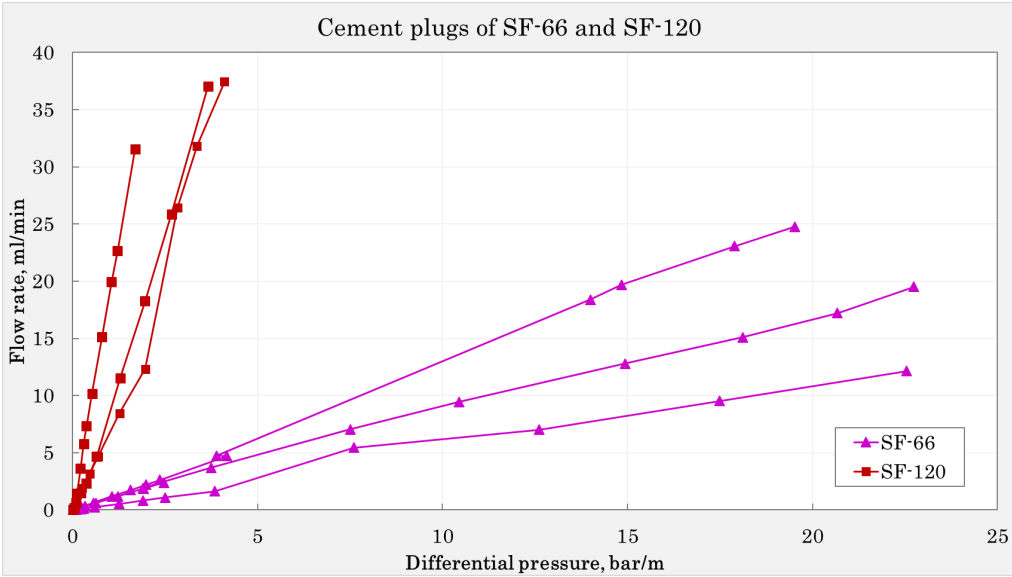

Figure 7. Results of samples SF-66 and SF-120

In our experiment, faster cement hydration and pozzolan reaction was expected in samples SF-120, therefore, the contraction at the cement/casing interface would be greater than that in samples SF-66. Consequently, the microannuli at the interface could be affected either by: (a) increase in the connectivity of the debonded sections, or (b) increase in the averaged width. This explained the high leak rate in the tests.

Effect of expanding agent

In general, samples of SF-120 with expanding agent produced an extremely small leak rate, less than 0.25 ml/min at the maximum differential pressure (20 bar). For comparison, leak rates from samples SF-120 without expanding agent were extrapolated linearly, and the average leak rate of these samples is 127.3 ml/min at 10 bar/m. With addition 2% of expanding agent, the leak rate was reduced considerably to 0.12 ml/min at 10 bar/m. Visual inspection to locate leak source was conducted in a similar method as described in the previous discussion. No visible continuous flow of gas bubble was observed at the surface of samples. The large reduction in leak rate and the absence of gas bubbles in visual inspection indicated that the microannuli was reduced significantly by adding an expanding agent.

The largely improved sealing performance of the expanding cement was due to the presence of magnesium oxide, which was the main component of the current expanding agent. The expansion in cement body was due to the internal pressure exerted upon the formation of a crystal of magnesium hydroxide on the surface of the cement matrix. This internal pressure can displace cement components to a certain extent and counteracts the natural condition of cement shrinkage upon setting. Several past studies have also proven the improvement in sealing from expanding cement, in term of reduction in microannuli size and water permeability [4, 11], and an increase in bond strength [25, 26].

CONCLUSION

On the basis of the current small-scale laboratory study conducted on cement plug made of silica cement systems, the following conclusions can be drawn:

- Cement plugs cured at elevated temperature has a reduced sealing performance. High curing temperature promotes cement shrinkage that is unfavorable for cement sealing properties. This shrinkage can also be enhanced due to the presence of silica flour in the cement mixture.
- Addition of expanding agent to silica cement increases the sealing performance of the cement plug as indicated by the considerable reduction of gas leak rate.

NOMENCLATURE

BWOC	= by weight of cement
API	= America Petroleum Institute
Ra	= roughness average

ACKNOWLEDGMENTS

The authors would like to thank the Research Council of Norway, Aker BP, ConocoPhillips, Equinor, and Wintershall for financing the work through the research center The Drilling and Well Centre for Improved Recovery (DrillWell). The authors would also like to thank Halliburton for providing the expanding agent.

REFERENCES

[1] NORSOK *NORSOK Standard D-010, Well Integrity in Drilling and Well Operations*, Rev. 4. Norway: Standards Norway (2013).

[2] Vrålstad, T., Saasen, A., Fjær, E., Øia, T., Ytrehus, J.D. and Khalifeh, M. "Plug & Abandonment of Offshore Wells: Ensuring Long-Term Well Integrity and Cost-Efficiency." *Journal of Petroleum Science and Engineering* Vol. 173 (2019): pp.478–491. DOI https://doi.org/10.1016/j.petrol.2018.10.049.

[3] Watson, T.L. and Bachu, S. "Evaluation of the Potential for Gas and CO2 Leakage along Wellbores." *E&P Environmental and Safety Conference*. SPE-106817-MS, January 1, 2007. 10.2118/106817-MS.

[4] Aas, B., Sørbø, J., Stokka, S., Saasen, A., Statoil, R.G., Lunde, Ø., Phillips, C. and Vrålstad, T. "Cement Placement With Tubing Left In Hole During Plug And Abandonment Operations." *IADC/SPE Drilling Conference and Exhibition*. SPE-178840-MS, March 1, 2016. 10.2118/178840-MS.

[5] Patchen, F.D. "Reaction and Properties of Silica-Portland Cement Mixtures Cured At Elevated Temperatures." *Petroleum Transactions, AIME* Vol. 219 (1960): pp.281–287.

[6] Nelson, E.B. and Barlet-Gouédard Thermal Cements. *Well Cementing*. Schlumberger. 319–342.

[7] Grabowski, E. and Gillott, J.E. "Effect of Replacement of Silica Flour with Silica Fume on Engineering Properties of Oilwell Cements at Normal and Elevated Temperatures and Pressures." *Cement and Concrete Research* Vol. 19 No. 3 (1989): pp.333–344. DOI 10.1016/0008-8846(89)90023-9.

[8] Gaurina-Međimurec, N., Sedić, K., Čajić, A. and Matijević, A. "Effect of Microblock on the Compressive Strength of Portland Cement at Elevated Temperatures." *ASME 2017 36th International Conference on Ocean, Offshore and Arctic Engineering*. OMAE2017-62455. Trondheim, Norway, June 25, 2017. 10.1115/OMAE2017-62455.

[9] Nelson, E.B. and Eilers, L.H. "Cementing Steamflood and Fireflood Wells-Slurry Design." *Journal of Canadian Petroleum Technology* Vol. 24 No. 05 (1985). DOI 10.2118/85-05-06.

[10] Peterson, B. "Bond of Cement Compositions for Cementing Wells." *6th World Petroleum Congress*. WPC-10123. Frankfurt am Main, Germany, June 19, 1963.

[11] Nagelhout, A., Bosma, M.G.R., Mul, P., Krol, G., van Velzen, H., Joldersma, J., James, S.G., Dargaud, B., Schreuder, R. and Théry, F. "Laboratory ond Field Validation of A Sealant System for Critical Plug-and-

Abandon Applications." *SPE Drilling & Completion* Vol. 25 No. 03 (2010): pp.314–321. DOI 10.2118/97347-PA.

[12] van Eijden, J., Cornelissen, E., Ruckert, F. and Wolterbeek, T. "Development of Experimental Equipment and Procedures to Evaluate Zonal Isolation and Well Abandonment Materials." *SPE/IADC Drilling Conference and Exhibition*. The Hague, Netherlands, March 14, 2017. 10.2118/184640-MS.

[13] Oil & Gas UK. *Guidelines on Qualification of Materials for the Abandonment of Wells*. Oil & Gas UK, Great Britain (2015).

[14] Opedal, N., Corina, A.N. and Vrålstad, T. "Laboratory Test On Cement Plug Integrity." *ASME 2018 37th International Conference on Ocean, Offshore and Arctic Engineering*. Madrid, Spain, June 17, 2018. 10.1115/OMAE2018-78347.

[15] Corina, A.N., Opedal, N., Vrålstad, T. and Sangesland, S. "A Laboratory Study Of The Effect Of Casing Pipe Roughness To Cement Plug Integrity." *SPE/IADC Drilling Conference and Exhibition*. SPE-194158-MS. The Hague, Netherlands, March 5, 2019.

[16] American Petroleum Institute. *API RP 10B-2: Recommended Practice For Testing Well Cements*. American Petroleum Institute, USA (2013).

[17] Opedal, N., Todorovic, J., Torsaeter, M., Vralstad, T. and Mushtaq, W. "Experimental Study on the Cement-Formation Bonding." *SPE International Symposium and Exhibition on Formation Damage Control*. SPE-168138-MS. Lafayette, Louisiana, USA, February 26, 2014. 10.2118/168138-MS.

[18] Torsæter, M., Todorovic, J. and Lavrov, A. "Structure And Debonding At Cement–Steel And Cement–Rock Interfaces: Effect Of Geometry And Materials." *Construction and Building Materials* Vol. 96 (2015): pp.164–171. DOI 10.1016/j.conbuildmat.2015.08.005.

[19] De Andrade, J., Sangesland, S., Skorpa, R., Todorovic, J. and Vrålstad, T. "Experimental Laboratory Setup For Visualization And Quantification Of Cement-Sheath Integrity." *SPE-173871-PA* (2016). DOI 10.2118/173871-PA.

[20] Wu, L., Farzadnia, N., Shi, C., Zhang, Z. and Wang, H. "Autogenous Shrinkage of High Performance Concrete: A Review." *Construction and Building Materials* Vol. 149 (2017): pp.62–75. DOI 10.1016/j.conbuildmat.2017.05.064.

[21] Jensen, O.M. and Hansen, P.F. "Influence Of Temperature on Autogenous Deformation and Relative Humidity Change in Hardening Cement Paste." *Cement and Concrete Research* Vol. 29 No. 4 (1999): pp.567–575. DOI 10.1016/S0008-8846(99)00021-6.

[22] Chu, I., Kwon, S.H., Amin, M.N. and Kim, J.-K. "Estimation of Temperature Effects on Autogenous Shrinkage of Concrete by a New Prediction Model." *Construction and Building Materials* Vol. 35 (2012): pp.171–182. DOI 10.1016/j.conbuildmat.2012.03.005.

[23] Zhang, W., Zhang, Y., Liu, L., Zhang, G. and Liu, Z. "Investigation Of The Influence Of Curing Temperature And Silica Fume Content On Setting And Hardening Process Of The Blended Cement Paste By An Improved Ultrasonic Apparatus." *Construction and Building Materials* Vol. 33 (2012): pp.32–40. DOI 10.1016/j.conbuildmat.2012.01.011.

[24] Maruyama, I. and Teramoto, A. "Temperature Dependence of Autogenous Shrinkage of Silica Fume Cement Pastes With a Very Low Water–Binder Ratio." *Cement and Concrete Research* Vol. 50 (2013): pp.41–50. DOI 10.1016/j.cemconres.2013.03.017.

[25] Ghofrani, R. and Plack, H. "CaO- And/Or MgO-Swelling Cements: A Key For Providing A Better Annular Sealing?" *SPE/IADC Drilling Conference*. CaO- and/or MgO-Swelling Cements, January 1, 1993. 10.2118/25697-MS.

[26] Rubiandini R. S., R. "New Additive for Improving Shearbond Strength in High Temperature and Pressure Cement." *IADC/SPE Asia Pacific Drilling Technology*. , January 1, 2000. 10.2118/62750-MS.

[27] Ametek. *Exploring Surface Texture: A Fundamental Guide to the Measurement of Surface Finish*. Taylor Hobson, Great Britain (2011).

ANNEX A
GAS FLOW RATE CORRECTION

Flowmeters installed in the setup measure the mass flow rate of gas at standard condition (pressure of 1 atm and temperature of 20° C). Because they are not sensitive to the change of pressure and temperature in the test cell, a correction of the volumetric flow rate is required. The average volumetric flow rate of nitrogen flowing through the cement plug, Q_{Av}, is calculated as follows:

$$Q_{AV} = Q \cdot \frac{P_S}{P_I} \cdot \frac{T}{T_S} \quad \text{(A-1)}$$

where:

Q_{AV} = average volumetric flow rate of nitrogen at inlet pressure and temperature during testing, m^3/s,
Q = flow of nitrogen into the specimen at STP[1] from the flowmeter, m^3/s,
P_I = inlet pressure, Pa,
P_S = reference pressure at STP, Pa,
T_S = reference temperature at STP, Kelvin,
T = test temperature, Kelvin.

ANNEX B
PIPE ROUGHNESS MEASUREMENT

Surface roughness instrument

The instrument for surface roughness measurement was MarSurf PS10 (Figure B- 1). It contains a probe with a stylus to pick-up the roughness of the convex side of a pipe.

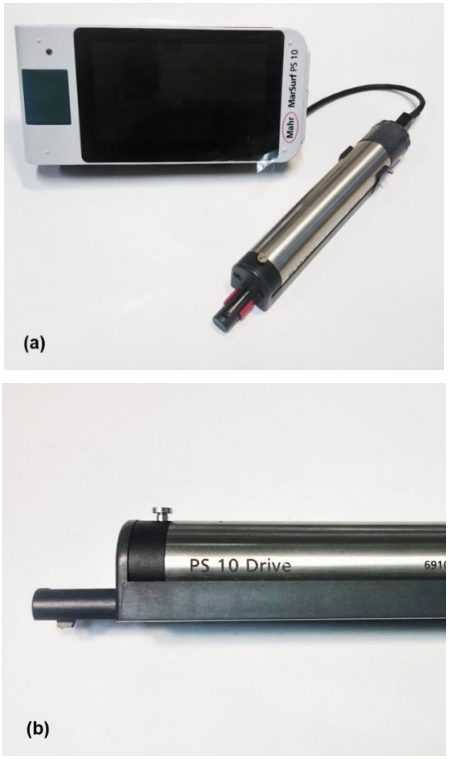

Figure B- 1. MahrSurf PS 10 Drive

Ra parameter

The roughness average (Ra) is the most commonly used parameter to describe surface roughness. Ra is the arithmetic average of the absolute ordinate values Z_i within the sampling length (Figure B-2), expressed mathematically as:

$$R_a = \frac{1}{n}\sum_{i=1}^{n}|Z_i| \quad \text{(B-2)}$$

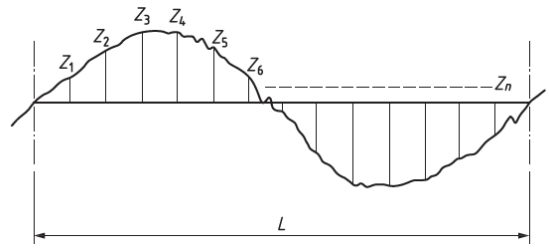

Figure B- 2. Illustration of Ra calculation [28]

[1] STP stands for the standard pressure and temperature at which the flowmeter is calibrated. Typically, the pressure is 1.013 x 10^5 Pa (1 atm) and the temperature is 20° C.

Appendix D

Paper III

Anisa Noor Corina, Nils Opedal, Torbjørn Vrålstad, Ragnhild Skorpa, Sigbjørn Sangesland

The Effect of Casing Pipe Roughness on Cement Plug Integrity

This paper was accepted by SPE Drilling and Completion on 24 September 2019.

Appendix D
Paper III

This paper is not included due to copyright
available at https://doi.org/10.2118/194158-PA

Appendix E

Paper IV

Anisa Noor Corina, Ragnhild Skorpa, Sigbjørn Sangesland, Torbjørn Vrålstad

Fluid Flow Analysis of Different Fluid Types Flowing Through Real Microannuli

This paper will be submitted for journal publication.

Appendix E
Paper IV

This paper is awaiting publication and is not included in NTNU Open

ISBN 978-82-326-4423-0 (printed version)
ISBN 978-82-326-4427-8 (electronic version)
ISSN 1503-8181

Doctoral theses at NTNU, 2020:30

Anisa Noor Corina

Cement Plug Integrity for Well Abandonment

NTNU
Norwegian University of
Science and Technology
Faculty of Engineering
Department of Geoscience and Petroleum

NTNU
Norwegian University of
Science and Technology

Doctoral Thesis

Anisa Noor Corina

Doctoral theses at NTNU, 2020:30

NTNU

NTNU
Norwegian University of
Science and Technology